

## Variability of USA East Coast surface total alkalinity distributions revealed by automated instrument measurements

Christopher W. Hunt <sup>a,\*</sup>, Joseph E. Salisbury <sup>a</sup>, Douglas Vandemark <sup>a</sup>, Steffen Aßmann <sup>b</sup>, Peer Fietzek <sup>c</sup>, Christopher Melrose <sup>d</sup>, Rik Wanninkhof <sup>e</sup>, Kumiko Azetsu-Scott <sup>f</sup>

<sup>a</sup> Ocean Process Analysis Laboratory, University of New Hampshire, Durham, NH, USA

<sup>b</sup> Kongsberg Maritime Contros GmbH, Kiel, Germany

<sup>c</sup> Kongsberg Maritime GmbH, Hamburg, Germany

<sup>d</sup> NOAA Northeast Fisheries Science Center, Narragansett, RI, USA

<sup>e</sup> NOAA Atlantic Oceanographic and Meteorological Laboratory, Miami, FL, USA

<sup>f</sup> Fisheries and Oceans, Canada, Bedford Institute of Oceanography, Dartmouth, NS, Canada

### ARTICLE INFO

#### Keywords:

Total alkalinity

Atlantic Ocean

USA

East Coast

Surface water

Coastal

### ABSTRACT

Seawater total alkalinity (TA) is one important determinant used to monitor the ocean carbon cycle, whose spatial distributions have previously been characterized along the United States East Coast via discrete bottle samples. Using these data, several regional models for TA retrievals based on practical salinity (S) have been developed. Broad-scale seasonal or interannual variations, however, are not well resolved in these models and existing data are highly seasonally biased. This study reports findings from the first long duration deployment of a new, commercially available TA titrator aboard a research vessel and the continuous underway surface TA measurements produced. The instrument, operated on seven East Coast USA cruises during six months in 2017 and for two months in 2018 on the summertime East Coast Ocean Acidification survey (ECOA-2), collected a total of nearly 11,000 surface TA measurements. Data from these efforts, along with a newly synthesized set of more than 11,000 regional surface TA observations, are analyzed to re-examine distributions of TA and S along the United States East Coast. Overall, regional distributions of S and TA generally agreed with prior findings, but linear TA:S regressions varied markedly over time and deviated from previously developed models. This variability is likely due to a combination of biological, seasonal, and episodic influences and indicates that substantial errors of  $\pm 10\text{--}20 \mu\text{mol kg}^{-1}$  in TA estimation from S can be expected due to these factors. This finding has likely implications for numerical ecosystem modeling and inorganic carbon system calculations. New results presented in this paper provide refined surface TA:S relationships, present more data in space and time, and improve TA modeling uncertainty.

### 1. Introduction

The important role of ocean alkalinity in regulating climate has become more apparent in recent years, as oceans are estimated to have absorbed about 25% of anthropogenic carbon dioxide (CO<sub>2</sub>) between 2006 and 2015 (Friedlingstein et al. 2019). Waters containing higher alkalinity concentration relative to CO<sub>2</sub> provide enhanced buffering and CO<sub>2</sub> sequestration potential. This sequestration has led to a decrease in global upper ocean pH by about 0.002 yr<sup>-1</sup> (Feely et al. 2004; Doney et al. 2011), a process termed ocean acidification (OA). Vast stores of alkalinity in deep ocean waters represent more than enough neutralizing

capacity to mitigate anthropogenic OA over millennial time scales (Zeebe 2012). Over decadal time scales, the less-buffered upper ocean and coastal waters, where high biological production occurs, are more susceptible to OA and its consequences. Coastal areas may be especially vulnerable to the impacts of OA (Mathis et al. 2015; Breitburg et al. 2015), but the dynamics of OA and buffering capacity in these areas are still poorly understood relative to the open ocean. This is due to the complex interplay between a number of additional coastal biogeochemical and physical processes, including biological calcium carbonate production and dissolution (Cross et al. 2013), anaerobic alkalinity generation (Thomas et al. 2009), river inputs (Salisbury et al. 2008),

\* Corresponding author.

E-mail address: [chunt@unh.edu](mailto:chunt@unh.edu) (C.W. Hunt).

intertidal marsh exchanges (Wang et al. 2016), bottom-water acidification from metabolic CO<sub>2</sub> accumulation (Cai et al. 2011; Mucci et al. 2011), as well as cross-shelf exchange (Chen and Wang 1999). These processes, combined with the large range of variability in coastal ocean alkalinity, pH, and hydrography, can lead to substantial uncertainties in ecosystem models used to predict future OA impacts in these areas (Wallace et al. 2014; Hagens et al. 2015; Breitburg et al. 2015).

TA and dissolved inorganic carbon (DIC) distributions along the United States East Coast ocean margin (henceforth shortened to East Coast) have been extensively studied during several transects, including the four GOMECC (Gulf of Mexico and East Coast Carbon) and ECOA (East Coast Ocean Acidification) cruises (Cai et al. 2010; Wang et al. 2013; Wanninkhof et al. 2015) and the Ocean Margins Program in the MAB (Chipman et al. 1995). These ongoing surveys provide a synoptic view of conditions in the region, but they were confined to the summer season, were resource- and labor-intensive, and were spaced several years apart. Methods that can expand temporal and spatial coverage of inorganic carbon system parameters would greatly enhance model estimates of East Coast DIC and CO<sub>2</sub> exchange (Signorini et al. 2013).

Recent developments in both ocean observation and data synthesis efforts offer the promise of vastly improved East Coast TA and inorganic carbon estimates. In-situ data compilations such as GLODAP (Olsen et al. 2016; Key et al. 2015) provide extensive collections of in-situ TA, DIC, and pH measurements. These datasets have been used to construct statistical relationships between TA and practical salinity (hereafter referred to as "salinity" in this work and abbreviated as "S") and sometimes temperature for major ocean basins (Lee et al. 2006; Millero et al. 1998; Takahashi et al. 2014), smaller sub-basins (Takahashi et al. 2014; Jiang et al. 2014; Cross et al. 2013), and even segmented coastal areas (DeGrandpre et al. 1997; Cai et al. 2010; Joesoef et al. 2017). In particular, Millero et al. (1998) presented an 'Atlantic' relationship assembled using surface data from 60°S to 80°N, whereas Lee et al. (2006) presented a 'North Atlantic' relationship using data from 30°N to 80°N.

These relationships have been used to estimate TA from either in situ salinity observations, salinity climatologies (Zweng et al. 2019), or space-based satellite measurements (Signorini et al. 2013; Fine et al. 2017; Salisbury and Jönsson 2018; Land et al. 2019; Reul et al. 2020). Satellite missions offer the potential for synoptic salinity estimates over vast spatial scales (Salisbury et al. 2015; Grodsky et al. 2018), which can then be used to derive estimates of surface ocean TA. The statistical relationships used to produce these estimates are, however, regionally and temporally variable (e.g. Land et al. 2019; Cai et al. 2010; Li et al. 2020). An additional source of high-quality TA data for the USA East Coast, collected at a higher frequency than the three-to-five year interval of the previous GOMECC/ECOA cruises, could inform the temporally variable nature of regional relationships. Recent technological advances and development efforts have provided a commercially available tool for this purpose: an automated TA analyzer (the CONTROS HydroFIA® TA, -4H-JENA Engineering GmbH, Jena, Germany, formerly of Kongsberg Maritime Contros GmbH, Kiel, Germany, hereafter referenced as HydroFIA TA). Deployed aboard a ship of opportunity, the collected underway surface TA measurements allow us to re-examine regional TA distributions along the East Coast and test existing statistical models relating salinity to TA. Here, we evaluate the performance of the HydroFIA TA instrument on multiple cruises aboard a ship of opportunity, present recommendations for future deployments, compare findings to previous studies as well as to a newly-assembled database of historical East Coast TA measurements, and discuss how data collected during this effort help to inform our understanding of TA variability along the East Coast.

## 2. Methods

### 2.1. Study regions

This study reports on observations from four East Coast oceanographic regions: Gulf of Maine, Nantucket Shoals/George's Bank, Middle Atlantic Bight, and offshore Shelf Break Front (Fig. 1). Delineations of the boundaries between these regions follow the methods of Signorini et al. (2013) and Hofmann et al. (2008). The Gulf of Maine (GOM, Fig. 1) is a highly productive, semi-enclosed shelf sea, encompassing the area between Cape Cod in Massachusetts and the Canadian province of Nova Scotia. The area east of the Scotian shelf and also east of the more northern Newfoundland and Labrador shelf system is where the warm, salty, northeast-flowing Gulf Stream and the colder, fresher, southwest-flowing Labrador Current interact (Loder et al. 1998). GOM circulation is typically cyclonic, with upstream Scotian Shelf and Atlantic slope water entering the region through the Northeast Channel and across the western Scotian Shelf, following the Maine coast southward, and exiting the GOM around the eastern flank of George's Bank and the Great South Channel between the Nantucket and George's Bank shoals. The area of George's Bank and Nantucket Shoals (GBN) comprises two shallow regions which together geographically separate the GOM from the Middle Atlantic Bight, bisected north-to-south by the Great South Channel. This region supports an active commercial fishery. The Middle Atlantic Bight (MAB) extends roughly from Cape Cod in Massachusetts to Cape Hatteras in North Carolina. This area also resides at the intersection of two major ocean currents: the colder, fresher inshore modified Labrador coastal current from the north (flowing first through the GOM and GBN regions) and the warmer, saltier offshore Gulf Stream from the south (Wang et al. 2013). These two currents are separated by the inshore shelf areas and slope sea further offshore, which stretches from Cape Hatteras to the Grand Banks. Warm core rings, shed from the Gulf Stream into the slope sea, are a frequent source of warm, high salinity water to the MAB region via cross-shelf exchange (Hofmann et al. 2008). The MAB is characterized by springtime phytoplankton blooms and low pCO<sub>2</sub> during the winter and spring months (DeGrandpre et al. 2002; Wang et al. 2013). The offshore Shelf Break Front (SBF) region delineates a band of slope sea stretching from south of Cape Hatteras northeastward nearly to Nova Scotia, encompassing the area where the seafloor deepens from several hundred meters to more than 2000 m, and forming a boundary region between the inshore GOM, GBN and MAB regions and the offshore slope sea.

### 2.2. Analytical methods for practical salinity, water temperature, and pCO<sub>2</sub>

Measurements in 2017 were collected on seven cruises of opportunity aboard the National Oceanic and Atmospheric Administration (NOAA) Ship *Henry B. Bigelow* (hereafter referred to as the *Bigelow*), a 64-meter fisheries research vessel. A summary of these cruises is provided in Table 1. Surface seawater temperature and practical salinity (hereafter referred to as salinity) were measured from a continuous surface seawater supply (intake depth about 3 m) using a Seabird SBE-45 thermosalinograph (Sea-bird Electronics, Bellevue WA, manufacturer precision of  $\pm 0.0001$  °C and  $\pm 0.0002$ , respectively). Measurements of the partial pressure of carbon dioxide (pCO<sub>2</sub>) were made from the same continuous surface seawater supply using a General Oceanics (Miami, FL) pCO<sub>2</sub> measurement system operated by the NOAA Atlantic Oceanography and Meteorological Laboratory (AOML), with a measurement accuracy of 2  $\mu$ atm, as detailed in Pierrot et al. (2009).

### 2.3. Discrete TA sample collection and analysis methods

Discrete samples for independent instrument evaluation were collected from the ship's underway seawater supply on two cruises and analyzed by two laboratories. Samples from Cruise 1 in 2017 were

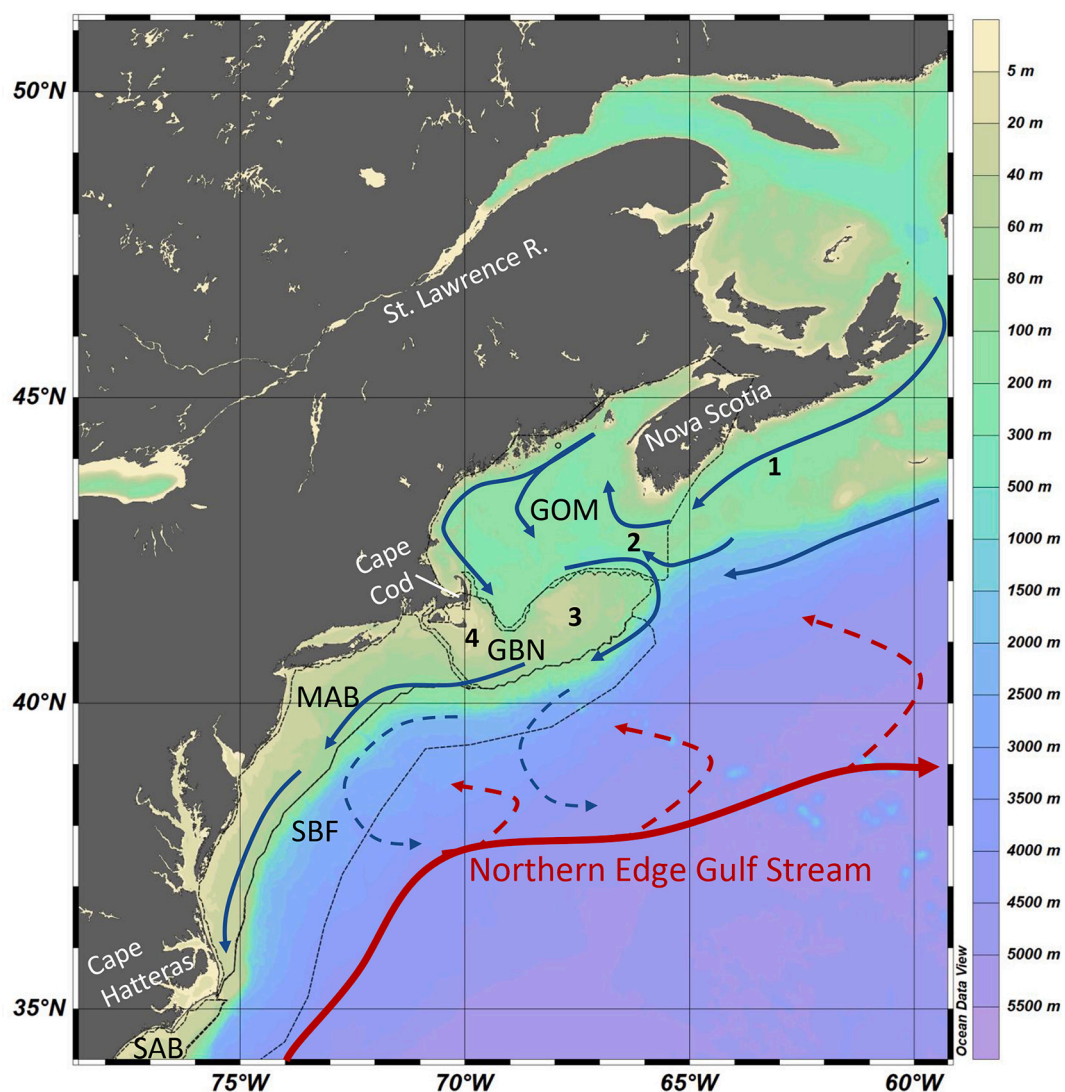


**Fig. 1.** Study area map with bathymetry, adapted from Townsend et al. (2006), with study subregions outlined. The study subregions are the Gulf of Maine (GOM), George's Bank/Nantucket Shoals (GBN), Middle Atlantic Bight (MAB), and Shelf-Break Front (SBF). The South Atlantic Bight (SAB) region is also shown south of Cape Hatteras. Numbers indicate specific locations found in the text: 1: Scotian Shelf; 2: Northeast Channel; 3: George's Bank; 4: Great South Channel. General positions of major currents are shown as red and blue arrows. The position of the Gulf Stream's northern edge is approximate, dashed red and blue arrows show the presence of cross-shelf mixing and not locations of actual currents. (For interpretation of the references to colour in this figure legend, the reader is referred to the web version of this article.)

**Table 1**  
Cruise summaries for the 2017 and ECOA-2 efforts, all aboard the NOAA Ship *Henry B. Bigelow*.

	Dates	Cruise Duration (days)	Latitude Range (°N)	Longitude Range (°W)	n TA observations	TA Range ( $\mu\text{mol kg}^{-1}$ )	Salinity Range	T Range (degrees C)
Cruise 1	Feb 11 - Feb 22, 2017	12	37.15–42.51	–75.67 - -65.42	1585	2136–2356	31.46–36.08	2.495–14.969
Cruise 2	Mar 7 - Mar 22, 2017	16	34.43–40.32	–76.29 - -72.76	1575	1888–2400	22.97–36.55	4.765–24.003
Cruise 3	Mar 28 - Apr 6, 2017	10	39.04–41.48	–74.01 - -70.51	1544	2068–2332	30.11–34.88	3.728–11.209
Cruise 4	Apr 12 - Apr 26, 2017	15	39.93–42.68	–71.38 - -65.76	1679	2171–2294	31.49–34.83	2.1483–11.211
Cruise 5	May 5–May 11, 2017	7	42.64–44.39	–70.74 - -66.57	536	2169–2217	31.2–32.52	4.504–8.167
Cruise 6	Jun 10 - Jun 22, 2017	13	40.62–44.23	–70.72 - -65.86	897	2156–2262	30.84–35.28	9.010–15.044
Cruise 7	Jul 6 - Jul 19, 2017	14	39.20–41.76	–73.38 - -65.27	1134	2156–2274	31.02–36.58	11.317–25.457
ECOA-2	Jun 26 - Jul 29, 2018	34	26.81–45.01	–80.98 - -61.4	1656	2001–2403	26.61–36.42	6.38–31.77

collected and analyzed by the NOAA Atlantic Oceanographic and Meteorological Laboratory (AOML). Samples during the 2018 ECOA-2 cruise were analyzed by the laboratory of Dr. Wei-Jun Cai (University of Delaware, referred to hereafter as U.Del.). Water from the shipboard seawater supply was transferred without bubbling into previously-flushed 500 ml (AOML) or 250 ml (U.Del.) glass BOD bottles with greased stoppers. These were filled to leave less than 1% headspace in the bottle. Samples analyzed by AOML were preserved with 200  $\mu$ l of saturated mercuric chloride solution and analyzed several weeks later; those analyzed by U.Del. were unpreserved and analyzed within 24 h. A detailed description of the AOML TA analysis is provided by [Barbero et al. \(2017\)](#), specific analysis details for AOML Cruise 1 samples are described by [AOML \(2020\)](#), and U.Del. methods are described by [Cai et al. \(2010\)](#). Briefly, each lab performed open-cell titrations, measuring the e.m.f. during titration via glass pH electrodes, with results calibrated via comparison to CRM. AOML titrations were performed with 0.2 N hydrochloric acid (HCl) prepared in a 0.55 m NaCl solution. U.Del. titrations were performed with 0.1 N HCl in a 0.5 m NaCl solution. The TA endpoint of the titrations were determined according to calculation of the Gran function ([Gran 1952](#)) with a nonlinear least squares correction for the presence of sulfate and fluoride ions ([Dickson et al. 2007](#)). AOML and U.Del. instrument performance statistics are discussed below and presented in [Table 2](#).

#### 2.4. Analytical method for underway total alkalinity

Total Alkalinity (TA) was measured using a CONTROS HydroFIA® TA analyzer ([Aßmann et al. 2013](#); [Seelmann et al. 2019](#)), modified for regular automated reference measurements as described below. [Seelmann et al. \(2019\)](#) provide a comprehensive account of instrument theory, design, and operation, and include extensive technical details we will not repeat here. Briefly, the HydroFIA TA instrument performs a single-point titration of seawater with 0.1 N hydrochloric acid prepared in deionized water, using brom cresol green (BCG) as the indicator for spectrophotometric pH detection, a technique developed by [Yao and Byrne \(1998\)](#) and refined by [Li et al. \(2013\)](#).

As part of the NOAA/OTT TAACT project (Tracking Ocean Alkalinity using New Carbon Measurement Technologies), the HydroFIA TA instrument was improved to allow for the automated, periodic

**Table 2**

Analytical uncertainties of paired discrete bottle sample and HydroFIA TA analyses. Paired sampling was conducted during Cruise 1 (Feb 11–22, 2017) and the 2018 ECOA-2 cruise. Discrete TA analyses were performed by two laboratories: the NOAA Atlantic Oceanographic and Meteorological Laboratory (“AOML”) and the laboratory of Dr. Wei-Jun Cai at the University of Delaware (“U.Del.”). AOML analyses used CRM Batches 129 and 144; U.Del. used Batch 173. The HydroFIA CRM was Batch 159 in 2017 and 173 during ECOA-2. AOML samples were preserved and analyzed three weeks after Cruise 1, U.Del. samples were not preserved and analyzed on board within 24 h of collection.

	2017 Cruise 1	ECOA-2
Analyzing laboratory	AOML	U.Del.
$\sigma$ (CRM)	$\pm 2.0$	$\pm 1.2$
RMSE (CRM)	$\pm 1.8$	$\pm 1.2$
$u_{(CRM)}$	$\pm 0.52$	$\pm 0.64$
$u_{(bias)_{CRM}}$	$\pm 1.9$	$\pm 1.4$
$u_c$	$\pm 2.8$	$\pm 1.8$
RMSE (rep)	$\pm 5.6$	$\pm 1.5$
$u_{(rep)}$	$\pm 5.2$	$\pm 0.9$
$n_{CRM,n_{rep}}$	10,9	81,27
$\sigma$ (HydroFIA CRM)	$\pm 2.0$	$\pm 1.4$
RMSE (HydroFIA CRM)	$\pm 1.3$	$\pm 3.8$
$u$ (HydroFIA CRM)	$\pm 0.59$	$\pm 0.64$
$u_{(bias)}$ HydroFIA	$\pm 1.4$	$\pm 3.9$
$u_c$ (HydroFIA)	$\pm 2.4$	$\pm 4.1$
$n$	9	25
RMSE, paired samples	$\pm 7.0$	$\pm 10.3$
$u_{(other)}$ , paired samples	$\pm 2.9$	$\pm 9.2$

measurement of certified reference material (CRM) by adding CRM input and exhaust ports, liquid switching valves, and a digital controlling device connected to an external computer (Supplementary Fig. S1). This capability is now a standard feature of the commercial version of the instrument. The CRM was obtained from the Scripps Institute of Oceanography laboratory of Dr. Andrew Dickson ([Dickson et al. 2003](#)), and its regular measurement supported assessments of instrument stability and accuracy over the course of multi-week deployments. Triplicate CRM measurements were typically made each day, while underway seawater TA measurements were made every 10–15 min. A customized software program controlled the HydroFIA TA instrument by switching between seawater and CRM sample streams, starting and stopping HydroFIA TA analysis, collecting salinity, water temperature, and location data from the ship’s centralized data system, supplying real-time salinity to the HydroFIA TA analyzer, and emailing data to shore-side researchers. The HydroFIA TA instrument was serviced by NOAA personnel between each cruise, who replaced the supplies of HCl and BCG, refilled the 2 l CRM reservoir (which was stoppered to limit evaporation), and re-calibrated the instrument with CRM. After these steps, the instrument was placed in standby mode until the *Bigelow* was underway, at which time a shipboard technician used the customized software program to begin data collection.

#### 2.5. Filtration of underway seawater for total alkalinity analysis

Unfiltered seawater was supplied to the HydroFIA TA instrument for the first five cruises. This resulted in a steady increase in pH readings and corresponding TA readings using the same batch of CRM, presumably due to fouling of the instrument’s optical cell. CRM absorbance spectra over these cruises showed decreased BCG absorbances at the isobestic point over time, which were closely correlated with increased CRM TA concentration. As the CRM TA concentration and volumes of BCG and HCl added did not change over time, we believe that accumulation of material on the optical cell resulted in increased absorbance at the indicator wavelengths. A blank spectrum measurement is made before BCG and HCl addition, and subtraction of this blank resulted in decreased calculated BCG absorbance as the blank absorbance increased. Drifts in the HydroFIA TA instrument have been observed by other investigators ([Seelmann et al. 2019](#)). CRM measurements from Cruises 1–5 showed clear, steady instrument drift of up to 93  $\mu$ mol kg<sup>-1</sup> by the end of Cruise 2, or a drift of nearly 3  $\mu$ mol kg<sup>-1</sup> per day (Supplementary Material Fig. S2, Table S1). After the fifth cruise an inline cross-flow filter (0.2  $\mu$ m) connected to a small 50 ml reservoir for filtered seawater was installed which eliminated the instrument drift during Cruises 6 and 7. The HydroFIA TA sample analysis time was 10 min, and flow rate supplied to the filter had to be adequate to replenish the reservoir within the analysis time frame. The cross-flow filter (currently supplied by 4H-JENA engineering GmbH, Jena, Germany, formerly Kongsberg Maritime Contros GmbH, Kiel, Germany) uses tangential flow filtration, where unfiltered seawater flowed continuously across the filter surface (in this case, a series of tubes of filter material) at positive pressure, with filtrate moving through the walls of the tubes and collected in a reservoir for analysis. This method allowed the same filter to be used for all subsequent cruises.

To account for instrument drift over the first five cruises, the differences between the CRM TA concentration and the mean of periodic triplicate instrument CRM readings were linearly interpolated; the interpolated CRM difference corresponding to each individual TA measurement was then retrieved from the HydroFIA TA timestamp and subtracted from the observed reading.

#### 2.6. Statistical calculations

In order to evaluate the performance of the HydroFIA TA instrument and reference titration systems from two laboratories, several statistical quantities were calculated following the approach of [Seelmann et al.](#)

(2019). Complete descriptions and equations are presented in the Supplementary Material. Briefly, five statistical parameters will be discussed. First, precision ( $\sigma$ ) was determined as one standard deviation of repeated measurements of certified reference material (CRM). Second, instrument accuracy (or also the uncertainty between two measurement methods, such as HydroFIA TA and laboratory TA measurements) was determined as the root mean square error (RMSE) of either repeated CRM measurements relative to the certified CRM TA or the difference between paired TA analyses. Third, the uncertainty in instrument bias,  $u$  ( $bias$ ), incorporates the instrument RMSE and the known uncertainty of the certified TA of the CRM. Fourth, the combined method uncertainty,  $u_c$ , incorporates  $u(bias)$  together with  $\sigma$ . Finally, the overall uncertainty between two TA measurement methods, such as HydroFIA TA and laboratory TA analyses, including factors such as replicate uncertainty and unknown uncertainties, is presented as  $u_c(HydroFIA\ TA, B)$ .

## 2.7. HydroFIA TA analyzer and discrete sample uncertainty evaluation

TriPLICATE periodic CRM measurements were automatically made on a roughly daily interval by the HydroFIA TA while underway during each cruise, permitting an assessment of precision ( $\sigma$ , Eq. 1). The CRM used in 2017 was Batch 159. For Cruises 1–5, the  $\sigma$  of triplicate CRM measurements ranged from  $\pm 0.2$  to  $\pm 9.2\ \mu\text{mol kg}^{-1}$ , with a mean  $\sigma$  of  $\pm 2.0\ \mu\text{mol kg}^{-1}$ . Addition of the filter resulted in no substantial change in the  $\sigma$  of CRM measurements for Cruises 6 or 7 in 2017 (mean CRM  $\sigma \pm 0.8$  and  $\pm 1.8\ \mu\text{mol kg}^{-1}$ , respectively). Accuracy of the HydroFIA TA during Cruises 1 through 7 in 2017, determined as the RMSE of periodic CRM readings which were corrected as described above, ranged from  $\pm 1.0$  to  $\pm 3.8\ \mu\text{mol kg}^{-1}$  with a mean value of  $\pm 2.2\ \mu\text{mol kg}^{-1}$ . These precision and accuracy levels matched or exceeded those given by the manufacturer ( $\pm 2$  and  $\pm 5\ \mu\text{mol kg}^{-1}$ , respectively).

Discrete TA samples were collected on two cruises from the same underway seawater supply sampled by the HydroFIA TA (Table 2). AOML measurements of CRM Batches 129 and 144 resulted in an uncertainty ( $u_c$ ) of  $\pm 2.8\ \mu\text{mol kg}^{-1}$ . Analysis of duplicate seawater samples returned an AOML sampling uncertainty,  $u(\text{rep})$ , of  $\pm 5.2\ \mu\text{mol kg}^{-1}$ . The RMSE of paired AOML-HydroFIA TA analyses was  $\pm 7.0$ ; solving Eq. 5 resulted in an estimated contribution of  $\pm 2.9\ \mu\text{mol kg}^{-1}$  of ‘other’ uncertainty to the total uncertainty between AOML and HydroFIA TA measurements, beyond the combined uncertainties of instrument precisions, biases, CRM uncertainties, and sampling or replicate uncertainties.

The calculations described above were used to compare HydroFIA TA results to those measured onboard by U.Del. during the 2018 ECOA-2 cruise (Table 2). U.Del. analyses of CRM Batch 173 showed a low overall method uncertainty ( $u_c$ ) of  $\pm 1.8\ \mu\text{mol kg}^{-1}$  and very good agreement between replicate samples, with a  $u(\text{rep})$  of  $\pm 0.9\ \mu\text{mol kg}^{-1}$ . Despite an overall HydroFIA TA  $u_c$  similar to that from Cruise 1 in 2017 ( $\pm 4.1\ \mu\text{mol kg}^{-1}$ , from triplicate measurements of CRM Batch 173), the RMSE between HydroFIA TA and U.Del. measurements was a relatively high  $\pm 10.3\ \mu\text{mol kg}^{-1}$ , with a  $u(\text{other})$  of  $\pm 9.2\ \mu\text{mol kg}^{-1}$ .

HydroFIA TA performance was consistent within  $\pm 2\ \mu\text{mol kg}^{-1}$  across cruises, making it challenging to attribute the difference in  $u(\text{other})$  between Cruise 1 in 2017 and ECOA-2. Possible factors contributing to  $u(\text{other})$  could be the choice to preserve (AOML) or not preserve (U.Del.) discrete samples, the timing of discrete sample collection relative to the intake of sample by the HydroFIA TA, nonlinearity of the HydroFIA TA instrument drift as documented by Seelman et al. (2019), or variable effects of the presence of titratable organic species dependent on the TA analysis method used. It is important to note that organic species represent an unknown but potentially significant contributor to TA (Yang et al. 2015; Kuliński et al. 2014; Fong and Dickson 2019). Neither the HydroFIA TA analyzer nor typical discrete TA titrations are capable of distinguishing organic alkalinity contributions, which may exert a variable influence depending on the acid-base characteristics of the organic species and the TA analysis method

employed (Sharp and Byrne 2020). This topic requires further examination, but for this work we will discuss TA as the inorganic system conforming to the definition set by Dickson (1981).

## 2.8. Data analysis

Linear regression analysis of salinity against TA was performed using an iteratively weighted least-squares algorithm with a bisquare weighting function (tuning constant 4.685) and robust fitting options enabled (*fitlm* in Matlab®, Mathworks, Natick MA USA). The robust fitting identified outliers as any point outside 1.5 times the interquartile above or below the 75th or 25th percentile, respectively, and outliers were excluded from the calculation of the  $r^2$  statistic. This outlier analysis excluded outliers at roughly the 10th and 90th percentiles. The regression analysis returned two linear coefficients: the change in TA per unit salinity (i.e. slope, designated “TA:S” hereafter) and the TA calculated at salinity zero (i.e. intercept, designated “TA<sup>0</sup>”). All regional and seasonal TA:S regressions were statistically unique according to one-way ANOVA tests, with  $p$ -values less than 0.05. Other studies (i.e. Lee et al. 2006) used a second-order polynomial regression with both salinity and temperature as independent input variables, but this approach yielded worse RMSE statistics for our data (results not shown), and we have chosen to use the linear regression approach described above. Data were divided into seasons according to the following: winter (December, January, February), spring (March, April, May), summer (June, July, August), and fall (September, October, November).

## 2.9. Historical data

To compare the results from this work to past observations in these regions, a historical dataset was assembled. Datasets used in this compilation included several categories: ship-of-opportunity measurements obtained from NOAA’s AOML, data from the GOMECC-1 and -2 and ECOA-1 East Coast surveys, newly-available data from Fisheries and Oceans, Canada (DFO), the global-scale GLODAPv2 (2019) synthesis product, and data from the Ocean Margins Project (OMP) in the MAB. The earliest TA observations made in the four study regions discussed in this work were from 1967, with the number of observations increasing steadily to the present, and with occasional years-long periods having no observations. The dataset contains over 11,000 surface measurements at depths of 10 m or less.

## 3. Results and discussion

HydroFIA TA measurements were collected on seven *Bigelow* cruises between February 11, 2017 and July 19, 2017 (Fig. 2), resulting in a total of 8950 surface seawater TA measurements (Table 1) and 167 CRM validation measurements. The same HydroFIA TA instrument used in 2017 aboard the *Bigelow* was also deployed during the 2018 ECOA-2 cruise, for 28 days in July and August 2018, collecting a total of 1656 TA and 75 CRM validation measurements. The 2018 ECOA-2 cruise occupied the same regions as the 2017 cruises (Fig. 2) and included a much more spatially comprehensive survey of the SAB region. To exploit the large number of new measurements made by the HydroFIA TA instrument, we examine the data obtained during the deployments aboard the *Bigelow* in the context of previously published analyses of TA distributions, and use these new observations to examine published relationships relating TA to sea surface salinity. We also re-evaluate data from other broad-scale data collections efforts in these regions. These comparisons are not meant to show that one dataset provides a better or worse understanding of TA conditions relative to another; rather, they are meant to show that TA conditions are dynamic in these coastal zones, and the capability provided by the largely unsupervised deployment of the HydroFIA TA system can help fill in knowledge gaps regarding seasonal and regional dynamics in ways that episodic research cruises collecting a necessarily limited number of discrete water samples

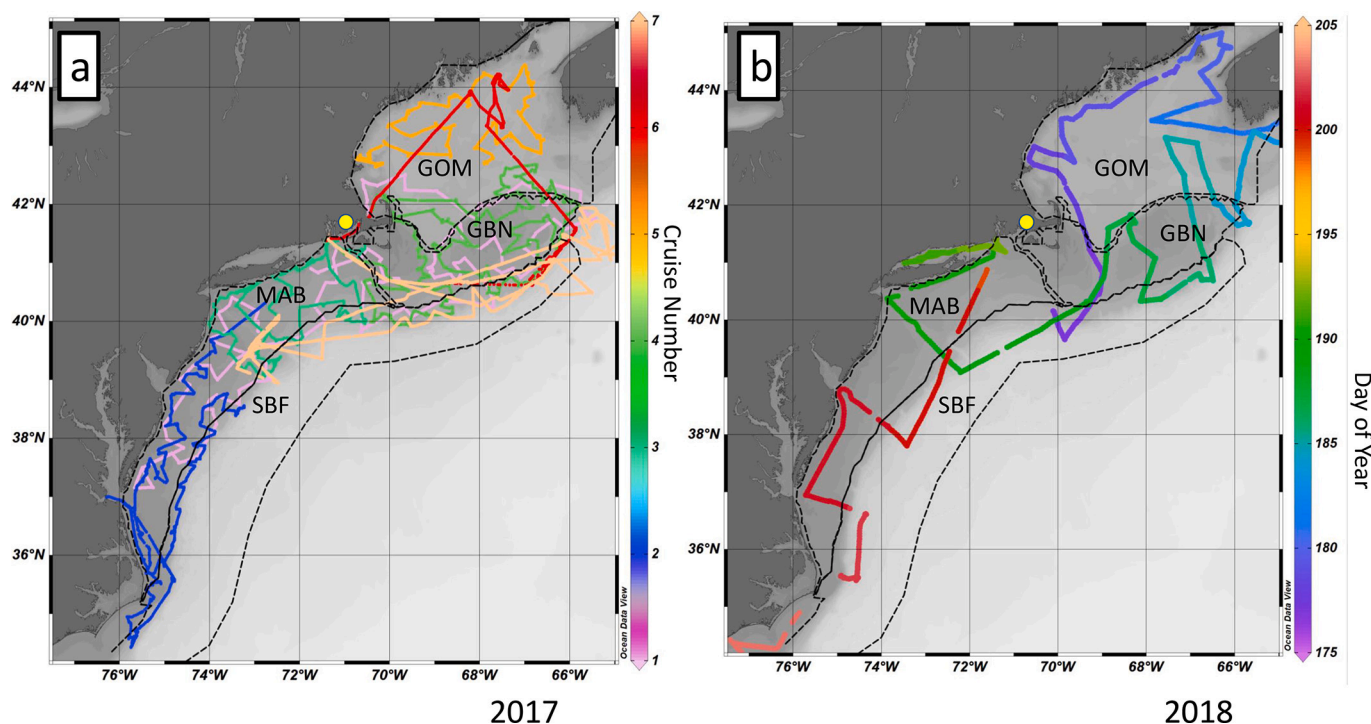


**Fig. 2.** Map of 2017 (panel a) and 2018 (panel b) cruise tracks presented in this work with East Coast regions outlined. Note that colors in panel a identify the cruise number (see Table 1), while colors in panel b indicate day-of-year. The NOAA Ship *Henry B. Bigelow*'s home port of Newport Rhode Island USA is shown as a yellow circle. A summary of these cruises is provided in Table 1. (For interpretation of the references to colour in this figure legend, the reader is referred to the web version of this article.)

cannot.

Salinity, water temperature, and TA generally increased from north to south in 2017, as upstream Scotian Shelf water feeds a coastal current flowing southward through the GOM and GBN regions to the MAB region, while gradually being modified by interactions with local rivers and offshore SBF water masses (Figs. 3 and 4, Table 3). Salinity and TA were lowest closer to shore and increased with distance from the coast in the GOM, GBN and MAB regions. The SBF region extends seaward from the outer boundary of each of the other regions, and was generally warmer, saltier, and higher in TA than the more shoreward regions. The SBF region contains a combination of slope water modified by interaction with the southward-flowing coastal shelf water along the boundary lines between the MAB, GBN and GOM regions (Dupont et al. 2006).

The increasing north-to-south trend in salinity, water temperature and TA was generally repeated in 2018, but the MAB region was an exception to this trend, as the MAB mean salinity ( $31.19 \pm 1.07$ ) and TA ( $2132 \pm 43 \mu\text{mol kg}^{-1}$ ) were both lowest among the studied regions. The ECOA-2 cruise made a shore stop in the MAB region, and the low-salinity data recorded outside the Newport News harbor mouth contributed to the low mean values (Xu et al. 2017). Nonetheless, even when these nearshore data are excluded the mean salinity and TA were still the lowest among the regions.

In contrast, seawater pCO<sub>2</sub> showed no clear regional pattern, and was almost always undersaturated or at near equilibrium with respect to the atmospheric CO<sub>2</sub> partial pressure (Table 3). Atmospheric pCO<sub>2</sub> measured by the shipboard AOML system averaged  $412 \pm 6 \mu\text{atm}$ . To test for significant differences among regional observations, we employed two-sample *t*-tests ('ttest2' in Matlab®, Mathworks Inc., Natick MA, USA), at a significance level (*p*) of 0.01. These tests showed that mean salinity, sea surface temperature, pCO<sub>2</sub> and TA were all statistically different between all regions in the 2017 dataset (Table 3). These differences are attributed to circulation patterns, variability of contributions from upstream or offshore water masses, terrestrial inputs, or biogeochemical processes; likely the variability is due to a

combination of all these factors. The same *t*-tests indicated that salinity, water temperature, TA and pCO<sub>2</sub> were all significantly different among the regions during ECOA-2.

### 3.1. Regional salinity:TA regressions

Regressions of regional HydroFIA TA data against salinity showed clear differences between years, regions, and seasons (Figs. 6-9). Broadly, the slope of the TA:S regression line for all 2017 data increased from the GOM ( $24.9 \pm 0.3$ ) to GBN ( $36.6 \pm 0.6$ ) to MAB ( $36.7 \pm 0.3$ ) regions along the path of southward-flowing coastal water, while TA<sup>0</sup> decreased from north to south ( $1395 \pm 8$ ,  $1011 \pm 19$ , and  $1008 \pm 11 \mu\text{mol kg}^{-1}$ , respectively). This pattern of increasing slope and decreasing TA<sup>0</sup> from north-to-south is consistent with the results of Cai et al. (2010), but the TA:S regression coefficients were distinctly different from those found by Cai et al. (2010) for all regions, with uniformly shallower slopes and higher TA<sup>0</sup>. The 2018 ECOA-2 data showed an opposite pattern to that from 2017, with decreasing TA:S slope from the GOM to GBN to MAB regions ( $62.7$ ,  $52.5$ ,  $38.5$ , respectively) and increasing TA<sup>0</sup> ( $178$ ,  $497$ ,  $936 \mu\text{mol kg}^{-1}$ , respectively). The regressions of surface TA against salinity were again distinctly different from those found by Cai et al. (2010) for all regions, with uniformly shallower slopes and higher TA<sup>0</sup> (Fig. 10), although the GOM slope ( $62.7$ ) and intercept ( $178 \mu\text{mol kg}^{-1}$ ) for 2018 were somewhat similar to the low-salinity GOM slope ( $65.8$ ) and TA<sup>0</sup> ( $75.1 \mu\text{mol kg}^{-1}$ ) from Cai et al. (2010). It is important to mention here that the TA-salinity relationships presented in Cai et al. (2010) were constructed from data acquired throughout the water column, from the surface to deeper slope and shelf waters, with the deepest samples ranging from 200 to 290 m. Thus, direct comparison between the surface measurements presented in this work and the deeper measurements used by Cai et al. (2010) may be unrealistic as contributions from various water masses are likely unequal.

Seasonal TA:S shifts were found in the GOM (Fig. 6). The 2017 winter TA:S slope ( $41.3$ ) and TA<sup>0</sup> ( $852 \mu\text{mol kg}^{-1}$ ) were similar to the high-

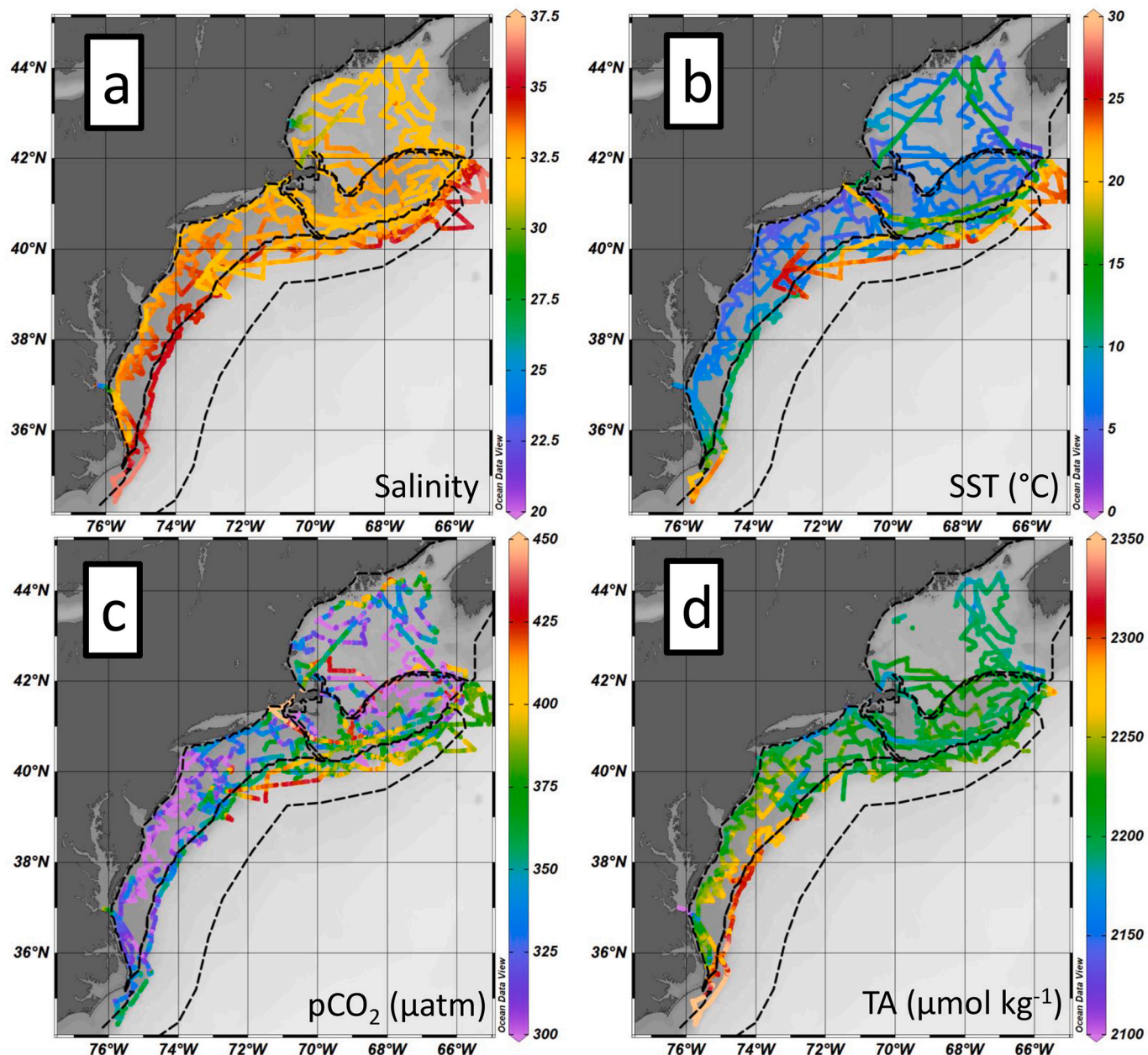


**Fig. 3.** Maps of all surface data collected underway in 2017. Parameters shown are sea surface salinity (panel a), temperature (panel b, degrees Celsius),  $p\text{CO}_2$  (panel c,  $\mu\text{atm}$ ), and HydroFIA TA (panel d,  $\mu\text{mol kg}^{-1}$ ). Black lines represent regional boundaries, see text and Fig. 1. Colour bars correspond to the data point colors in each panel and are scaled identically to those in Fig. 4.

salinity values of Cai et al. (2010, data collected in summer), who reported a slope and  $\text{TA}^0$  of 39.1 and  $932 \mu\text{mol kg}^{-1}$ , but during the springtime in 2017 (March through May) the GOM TA:S changed substantially, with a much shallower slope (24.3), higher  $\text{TA}^0$  (1415  $\mu\text{mol kg}^{-1}$ ), and lower  $r^2$  (0.77). These conditions persisted into the summer of 2017 (June and July) in the GOM, and contrast sharply with the GOM TA:S regression in the summer of 2018. A similar 2017 seasonal shift was seen in the GBN region (Fig. 7) from winter, through spring and into summer, with progressively shallower slopes (32.3, 30.2, and 18.4, respectively), higher  $\text{TA}^0$  (1160, 1215, 1600, respectively), and lower  $r^2$  (0.63, 0.63, 0.40, respectively).

Seasonal regressions from the MAB region in 2017 were lagged in time compared to those from the GOM and GBN regions. MAB winter and spring 2017 TA:S results were quite consistent in 2017 (Fig. 8), with similar TA:S slopes (40.8 and 44.1, respectively) and  $\text{TA}^0$  (880 and 763

$\mu\text{mol kg}^{-1}$ , respectively), and encompassed the MAB slope and  $\text{TA}^0$  provided by the historical dataset (43.7 and 769  $\mu\text{mol kg}^{-1}$ , respectively). The summer MAB regression changed substantially in a similar fashion to the GOM and GBN regions, with the TA:S slope dropping from 44.1 to 14.5 and  $\text{TA}^0$  increasing from 763 to 1726  $\mu\text{mol kg}^{-1}$ .

SBF TA:S regressions further reinforce the observation that a seasonal shift occurred, as SBF winter and spring slope (44.2 and 42.2, respectively) and  $\text{TA}^0$  (761 and 821  $\mu\text{mol kg}^{-1}$ , respectively) were similar in 2017, whereas the summer slope (21.7) and  $\text{TA}^0$  (1497  $\mu\text{mol kg}^{-1}$ ) were markedly different (Fig. 9). SBF results are also notably differentiated by latitude: Steeper SBF winter and spring slopes were influenced by data from latitudes at or below 39°N, whereas the shallower summer SBF slope was mostly controlled by data from latitudes higher than 40°N. Cruise tracks from 2017 (Fig. 2) showed that the SBF data north of 40°N were collected in a region near the confluence of the

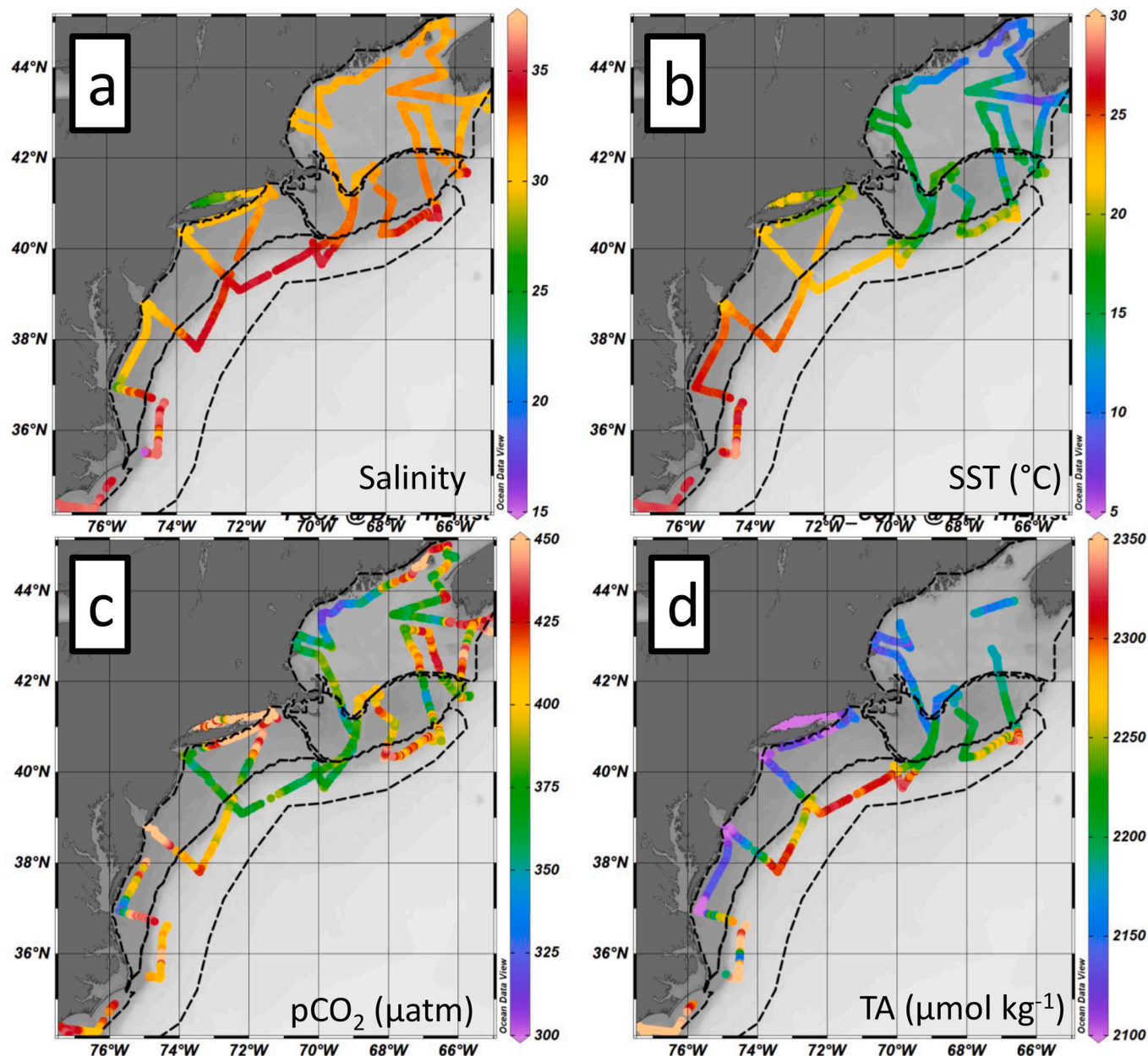


**Fig. 4.** Maps of ECOA-2018 sea surface salinity (panel a), temperature (panel b, degrees Celsius), pCO<sub>2</sub> (panel c,  $\mu\text{atm}$ ), and HydroFIA TA (panel d,  $\mu\text{mol kg}^{-1}$ ). Black lines represent regional boundaries, see text and Fig. 1. Colour bars correspond to the data point colors in each panel and are scaled identically to those in Fig. 3. The low-salinity, low-alkalinity data shown in Long Island Sound do not fall within the bounds of the regions discussed in this study, and thus do not influence the discussion of regional findings.

SBF, GOM, and MAB regions, whereas the cruise tracks south of 39°N ran very close to the boundaries between the SBF and MAB regions. The SBF slope from 2018 (46.9) was similar to the steeper, lower-latitude 2017 data group and the historical SBF slope (47.9). The 2018 SBF data also followed a uniform linear trend regardless of latitude.

The work of Lee et al. (2006) presented a polynomial expression of both salinity and sea surface temperature for the estimation of TA in North Atlantic surface waters, so direct comparison of linear regression coefficients is not possible here. The GOM equation of Cai et al. (2010) returned TA closer to measured values in 2017 (mean difference  $8 \pm 14 \mu\text{mol kg}^{-1}$ , Table 4) compared to the Lee et al. (2006) equation including in situ sea surface temperature (mean difference  $13 \pm 10 \mu\text{mol kg}^{-1}$ ). The reverse was true in the MAB region where the TA calculated according to Lee et al. (2006) was more similar to the observed HydroFIA TA values (mean difference  $1 \pm 12 \mu\text{mol kg}^{-1}$ ) than TA calculated from

the Cai et al. (2010) equation (mean difference  $12 \pm 16 \mu\text{mol kg}^{-1}$ ). The GBN region was represented equally well in 2017 by the Lee et al. (2006) equation (mean difference  $4 \pm 10 \mu\text{mol kg}^{-1}$ ) and Cai et al. (2010) equation (mean difference  $-5 \pm 16 \mu\text{mol kg}^{-1}$ ).

Regional and seasonal changes in TA:S combine to form a cohesive trend in 2017. During winter, the TA:S slope and TA<sup>0</sup> for all regions except the SBF were indistinguishable both from those of Cai et al. (2010, Figs. 6-9) and from historical TA:S trends (Fig. 10). The winter SBF slope (44.2), while not indistinguishable, still resembled the slope from the historical dataset (47.9) as well as the “Atlantic” slope of 51.2 presented by Millero et al. (1998, Fig. 9). Thus, the winter of 2017 data appear to reflect ‘typical’ conditions consistent with previous findings. In contrast, atypical conditions developed in the GOM in the spring of 2017 and continued into the summer and expanded southward and westward to the GBN, MAB, and SBF regions. By the summer of 2017, all

**Table 3**

Regional summary statistics for 2017 and ECOA-2 data. In order, the data presented for each parameter (e.g. salinity, temperature) are: the regional range of each observation type (minimum and maximum), the statistical mean, one standard deviation around the mean, and total number of measurements in each region. The mean, standard deviation, and measurement number are grouped in parentheses. Results from the 2018 ECOA-2 cruise are in shaded rows. Bold values indicate the highest and lowest values observed for each parameter in 2017 and 2018.

	Dates	Salinity	Temperature (degrees C)	pCO <sub>2</sub> (μatm)	TA (μmol kg <sup>-1</sup> )
GOM	Feb	<b>24.13</b> –33.68	2.87–14.54	229–448	2154–2258
	19 -	(31.95 ± 0.85	(8.30 ± 3.26 n	(335 ± 43	(2196 ± 15 n
	Jun	<i>n</i> = 2244)	= 2271)	<i>n</i> = 1546)	= 1857)
	21,				
GOM	Jun	30.94–32.34	<b>6.37</b> –18.91	310–457	2112–2213
	27 -	(31.72 ± 0.31	(13.17 ± 2.96	(390 ± 33	(2158 ± 18 n
	Jul 7,	<i>n</i> = 497)	<i>n</i> = 497)	<i>n</i> = 484)	= 185)
GBN	Feb	31.12–33.57	<b>2.15</b> –20.94	202–564	2166–2267
	16 -	(32.75 ± 0.42	(7.96 ± 3.87 n	(346 ± 54	(2211 ± 16 n
	Jul	<i>n</i> = 1451)	= 1460)	<i>n</i> = 1353)	= 1196)
	19,				
GBN	Jun	31.48–32.80	10.14–18.71	333–441	2146–2225
	26 -	(32.46 ± 0.33	(15.74 ± 1.87	(378 ± 16	(2204 ± 17 n
	Jul 8,	<i>n</i> = 212)	<i>n</i> = 212)	<i>n</i> = 201)	= 196)
MAB	Feb	28.99–35.04	<b>3.73</b> –25.45	255–599	<b>2087</b> –2400
	11 -	(32.98 ± 0.85	(9.18 ± 6.16 n	(331 ± 36	(2225 ± 31 n
	Jul	<i>n</i> = 3285)	= 3288)	<i>n</i> = 3009)	= 2699)
	19,				
MAB	Jul 8 -	<b>26.61</b> –33.47	17.85–26.28	<b>307</b> –534	<b>2001</b> –2257
	Jul	(31.19 ± 1.07	(22.23 ± 2.38	(421 ± 52	(2132 ± 43 n
	20,	<i>n</i> = 219)	<i>n</i> = 219)	<i>n</i> = 189)	= 193)
	2018				
SBF	Feb	<b>31.26</b> – <b>36.55</b>	4.85–25.19	<b>196</b> –437	2183–2397
	12 -	(33.76 ± 1.12	(13.57 ± 6.1 n	(352 ± 42	(2247 ± 44 n
	Jul	<i>n</i> = 2564)	= 2570)	<i>n</i> = 2353)	= 2116)
	18,				
SBF	Jun	<b>30.77</b> – <b>36.20</b>	<b>14.37</b> – <b>29.14</b>	352–480	2138–2389
	26 -	(34.08 ± 1.06	(22.49 ± 3.1	(398 ± 27	(2285 ± 50 n
	Jul	<i>n</i> = 353)	<i>n</i> = 353)	<i>n</i> = 325)	= 325)
	21,				
SBF	2018				

**Table 4**

Deviations between 2017 TA observations and TA estimates from regional models. The models used are those of Cai et al. (2010) and Lee et al. (2006). All differences are calculated as model-derived TA subtracted from the observed TA, thus positive values indicate model underestimate relative to the observed TA. Negative values are shown in parentheses. The third column (“Difference  $\sigma$ ”) lists one standard deviation of the calculated differences for each region, and the fourth column lists the number of observations. All values are  $\mu\text{mol kg}^{-1}$ .

Region	Difference from Cai et al. (2010)			
	Mean Difference	Range of Difference	Difference $\sigma$	n
GOM	8	(–33) - 74	14	1546
GBN	–5	(–52) - 90	16	1353
MAB	12	(–60) - 97	16	3009
SBF	–	–	–	–
Difference from Lee et al. (2006)				
Region	Mean Difference	Range of Difference	Difference $\sigma$	n
GOM	13	(–27) - 82	10	1539
GBN	4	(–32) - 67	10	1353
MAB	1	(–66) - 87	12	2764
SBF	–4	(–64) - 53	13	1919

regions showed TA:S conditions quite different from both the historical dataset and the results of Cai et al. (2010). These atypical summer conditions were not reflected in the 2018 ECOA-2 data, so the progression seen in 2017 is likely not due to typical seasonal patterns. Instead, the historical data show that the shifts in 2017 were opposite of the typical seasonal changes in TA:S slope and TA<sup>0</sup>.

### 3.2. Seasonal biases in data availability

It is important to note here the paucity of available historical TA observations in winter; despite collecting the broadest extent of data we could find, there were no surface TA measurements in any region in January, and only about 25 GOM measurements in December (Fig. 5). The vast majority of historical winter measurements were taken in February, and the existing East Coast TA data are overall heavily weighted towards summertime sampling. Data collected aboard the *Bigelow* in 2017 by the HydroFIA TA instrument provided some of the first widely spatially-distributed TA measurements along the East Coast outside the summer months, as the GOMECC and ECOA cruises were all conducted during the summer months of June, July and August. Regular NOAA Ecosystem Monitoring (EcoMon) cruises have been conducted since 2012 during non-summer months, including TA sampling, but with a limited number of stations. Incorporation of the data collected in this work increases available TA observations by more than one order of magnitude during the months when the HydroFIA TA system was deployed. Winter is a difficult time to conduct cruises in Atlantic waters, but it is also a biologically important season, as it sets up conditions for the springtime bloom. The lack of historical evidence of shifts in seasonal TA:S, such as we have shown, may not be because these shifts are rare, but because the data have not been available to detect them.

### 3.3. Mechanisms affecting linear TA:S relationships

A variety of processes can alter ocean TA and salinity, contribute to TA:S variability, and potentially contribute to the observations presented here. Over time scales greater than 100,000 years, alkalinity (and salinity) in the oceans are controlled by geologic weathering and net seafloor sedimentary processes whereas over time scales between 1000 and 100,000 years surface alkalinity is controlled by variations in biological pumping and interactions with carbonate and silici-clastic sediments (Zeebe 2012). On shorter time scales, Takahashi et al. (2014) described five “oceanographic situations” and their effect upon the linear TA:S relationship. These situations, which will be discussed in terms of their applicability to the findings from this study, are: (a) evaporation-precipitation (b) mixing in subtropical gyres between subtropical waters (whose TA is depleted by calcareous organism growth) and fresher subpolar waters enhanced in TA due to upwelling (c) biological production and decomposition, especially of CaCO<sub>3</sub>-containing shells (d) mixing of a source water with river water containing higher or lower TA, and (e) mixing of a source water with another body of water containing higher salinity and reduced TA (such as a warm evaporative basin or upwelled slope waters). As evaporation-precipitation (a) alters salinity and TA in proportion, this process will not affect the TA:S relationship. Neighboring regions exhibiting higher salinity and TA include the coastal SAB region to the south and the more offshore Gulf Stream water mass, providing two possible sources contributing to process (e). The regions in this study are likely not large enough to reflect changes in subtropical-subpolar mixing over seasonal time scales (e.g. Fry et al. 2015), and thus process (b) can be discounted. This leaves the situations of biological production (c), river water mixing (d), or mixing with a higher salinity water mass (e) as the most likely processes affecting the TA:S relationships in these regions.

### 3.4. The effect of net calcification or dissolution

CaCO<sub>3</sub> production events have been shown to lower TA (Bates et al.

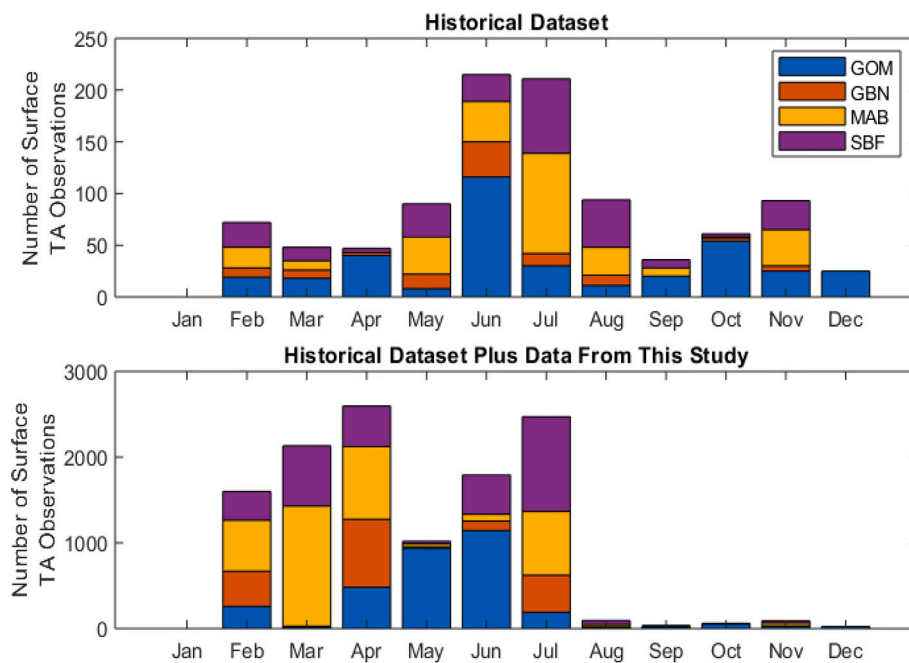


**Fig. 5.** Monthly counts of regional surface TA measurements. The top panel shows the counts for each region from the historical dataset described in Section 2.4. The bottom panel shows counts for each region once the HydroFIA TA system measurements from 2017 and 2018 described in this study are included. Note the roughly one order of magnitude difference in y-axis scales between top and bottom panels.

1996a; Bates 2001), and therefore alter the slope of the TA:S line. In a regional context, uniform production across the region would result in no change to the TA:S line, whereas higher production in the saltier waters of a region would lead to a decreased TA:S slope, and higher production in the lower salinity waters would lead to an increased slope. This biological utilization in high-nutrient waters can potentially account for up to a 50  $\mu\text{mol kg}^{-1}$  TA reduction (Takahashi et al. 2014; Bates et al. 1996b; Harley et al. 2010). It is conceivable that an offshore bloom of a calcifying species (such as a coccolithophore) could have drawn down TA in 2017, reducing the slope of the TA:S mixing line. This could explain the high-salinity data in 2017 that fall well below the Millero et al. (1998) regression line (Fig. 9), but corresponding  $\text{CaCO}_3$  dissolution is needed to explain the low-salinity data that fall above the Millero et al. (1998) line. This can be seen especially in the offshore SBF region, where the 2017 summertime TA:S line appears to be rotated about a salinity of 33 relative to the other SBF regression lines, with lower TA above salinity 33 and higher TA below (Fig. 9). An offshore calcifying bloom could explain the apparent TA drawdown above salinity 33, with corresponding  $\text{CaCO}_3$  dissolution inshore explaining the elevated TA input below salinity 33. Indeed, reductions in the TA:S slopes in the GOM, GBN and MAB regions all appear to be due to lower-salinity TA enhancement (Figs. 6-8).

The formation of  $\text{CaCO}_3$  by calcifying species results in elevated  $\text{pCO}_2$  through shifts in the DIC:TA ratio, with the opposite effect for  $\text{CaCO}_3$  dissolution (Zeebe 2012; Bates et al. 1996b); however, the overall net  $\text{pCO}_2$  change depends on the amount of  $\text{CaCO}_3$  formation or dissolution relative to net ecosystem production. Thus, elevated  $\text{pCO}_2$  levels would be expected in areas where calcification is the primary mechanism of TA:S variability, and reduced  $\text{pCO}_2$  in those areas where dissolution predominates, although other mechanisms may offset some or all of this  $\text{pCO}_2$  increase (Balch 2018). In the case of the GOM region, the mean 2017 summer  $\text{pCO}_2$  (335  $\mu\text{atm}$ ) was lower than any other sampling period within the GOM region for this study, a potential indication of  $\text{CaCO}_3$  dissolution, or alternatively high net productivity. For a historical climatological comparison all surface  $\text{pCO}_2$  measurements within each study region were extracted for each season from the 2019 Surface Ocean  $\text{CO}_2$  Atlas with data from 1957 to 2019

(SOCAT2019, Bakker et al. 2016). The mean GOM  $\text{pCO}_2$  in summer 2017 (336  $\mu\text{atm}$ ) was significantly lower than the historical (2002–2018) mean GOM summer  $\text{pCO}_2$  from the SOCAT database (370  $\mu\text{atm}$ ) as well as the mean GOM  $\text{pCO}_2$  from the 2018 ECOA-2 cruise (390  $\mu\text{atm}$ , significance determined according to one-way ANOVA tests, see Supplementary Material Fig. S3). Some of this difference may be due to the colder temperature in 2017 resulting in lower  $\text{pCO}_2$ . Furthermore, the 2017 summer MAB and SBF mean  $\text{pCO}_2$  values (376 and 366  $\mu\text{atm}$ , respectively) were significantly lower than the respective values from summer 2018 during the ECOA-2 cruise (421 and 398  $\mu\text{atm}$ , respectively) or seasonal mean  $\text{pCO}_2$  from the SOCAT database (411 and 392  $\mu\text{atm}$ , respectively). While the presence of lower  $\text{pCO}_2$  concurrent in space and time with the atypical TA:S relationships supports the idea that  $\text{CaCO}_3$  dissolution resulted in elevated TA:S slopes in the coastal GOM and MAB regions, this mechanism is unlikely given that these surface waters are typically supersaturated with  $\text{CaCO}_3$  (Wanninkhof et al. 2015).

### 3.5. Potential river or shelf mixing effects

Mechanisms (d), mixing of a source water with river water containing higher or lower TA and (e), mixing with a higher salinity water mass, remain as explanations to the observed seasonal TA:S shifts. Cai et al. (2010) characterized the GOM, GBN and MAB regions as “Current-Dominated Margins”, where freshwater and TA inputs from local rivers are greatly outweighed by those carried by alongshore currents. For regions in this study, the dominant alongshore current is the southward-flowing Labrador Current, a branch of which travels successively southward through the GOM, GBN, and MAB regions. Recent rapid warming of the Gulf of Maine (Pershing et al. 2015; Pershing et al. 2018) has been linked to increased intrusions of deeper, salty, and warm water through the Northeast Channel and concurrent reductions in Labrador water (Fig. 1, Townsend et al. 2015, Brickman et al. 2018), the prevalence of which are in turn affected by changes in the Atlantic Meridional Overturning Circulation (Sherwood et al. 2011; Claret et al. 2018) or changes in the strength of the Labrador Current inflows (Jutras et al. 2020). Cai et al. (2010) suggest that continuous mixing of regional

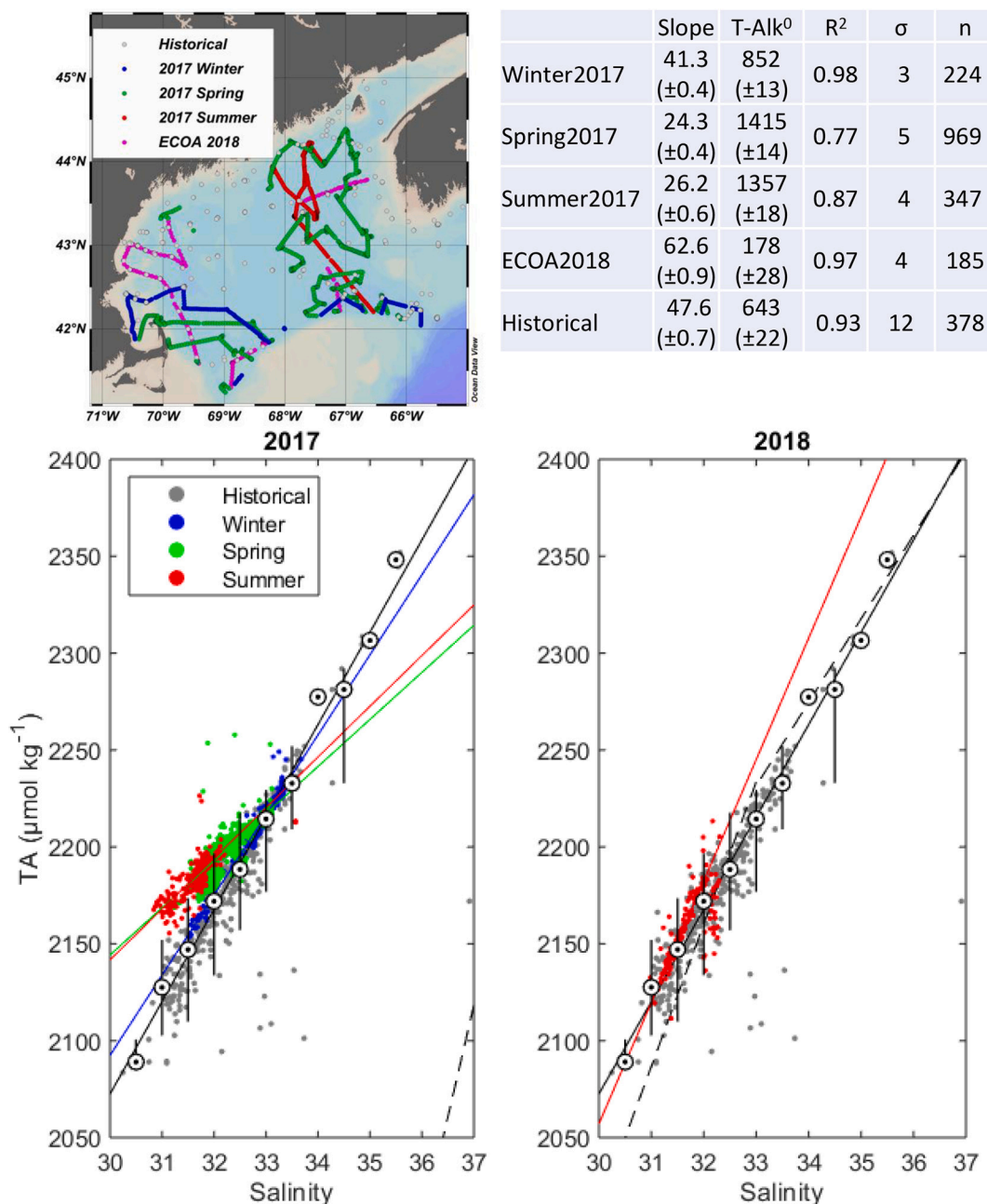


**Fig. 6.** Gulf of Maine seasonal and historic TA and salinity data. Upper-left panel shows the locations of surface data collections. Lower-left and lower-right panels show scatterplots of seasonal salinity and TA from 2017 and the 2018 ECOA-2 cruise, respectively. Note that the historical data are inclusive of all seasons. For reference, the solid line indicates the robust linear regression of historical data; the dashed lines indicate the mixing lines described by Cai et al. (2010). The slope and  $TA^0$  from Cai et al. (2010) are  $65.8$  and  $75.1 \pm 291.2 \mu\text{mol kg}^{-1}$ , respectively, for sample salinities less than  $31.75$ . The slope and  $TA^0$  from Cai et al. (2010) are  $39.1$  and  $932.7 \pm 16.5 \mu\text{mol kg}^{-1}$ , respectively, for sample salinities greater than  $31.75$ . Whisker plots show the median TA (white circles) at 0.5-salinity intervals of historical data; whiskers indicate the range of TA over each 0.5-salinity interval. Colored lines show the linear regression of measurements for each season. The table in the upper-right lists the linear regression slope and intercept coefficients (with standard errors in parentheses), as well as the  $r^2$ , RMSE and  $n$  statistics. The  $p$ -values for all regressions were much less than 0.01.

surface water with deeper slope and shelf waters would result in the lowering of the TA:S slope, providing a possible explanation of the seasonal shifts seen in this study. This explanation may not be satisfactory, as the regional salinities in 2017 generally decreased from winter to spring and then summer, while the TA at lower salinity gradually rises above the mixing line, suggesting a change in the amount of freshwater and TA being carried into the region.

The seasonal TA:S shifts seen in the 2017 data may have resulted from an increase of upstream shelf water entering the GOM relative to warm slope water. GOM temperature anomaly analyses, updated

through 2020 using methods described by Pershing et al. (2015), show that GOM surface temperatures in early 2017 (January and February) were high enough to be judged a ‘heat wave’ (Pershing et al. 2018, updated data presented at <https://www.gmri.org/stories/gulf-maine-temperature-update-normal-new-cold/>, accessed 10/4/2020). The GOM surface water temperature then fell through the spring and early summer to either lower-than-usual or typical values, indicating a transition from warmer, saltier source water to colder, fresher shelf water. Cai et al. (2010) report a Labrador TA:S regression slope of 33 and  $TA^0$  of  $1124 \mu\text{mol kg}^{-1}$ . These values are lower than the 2017 summer GOM

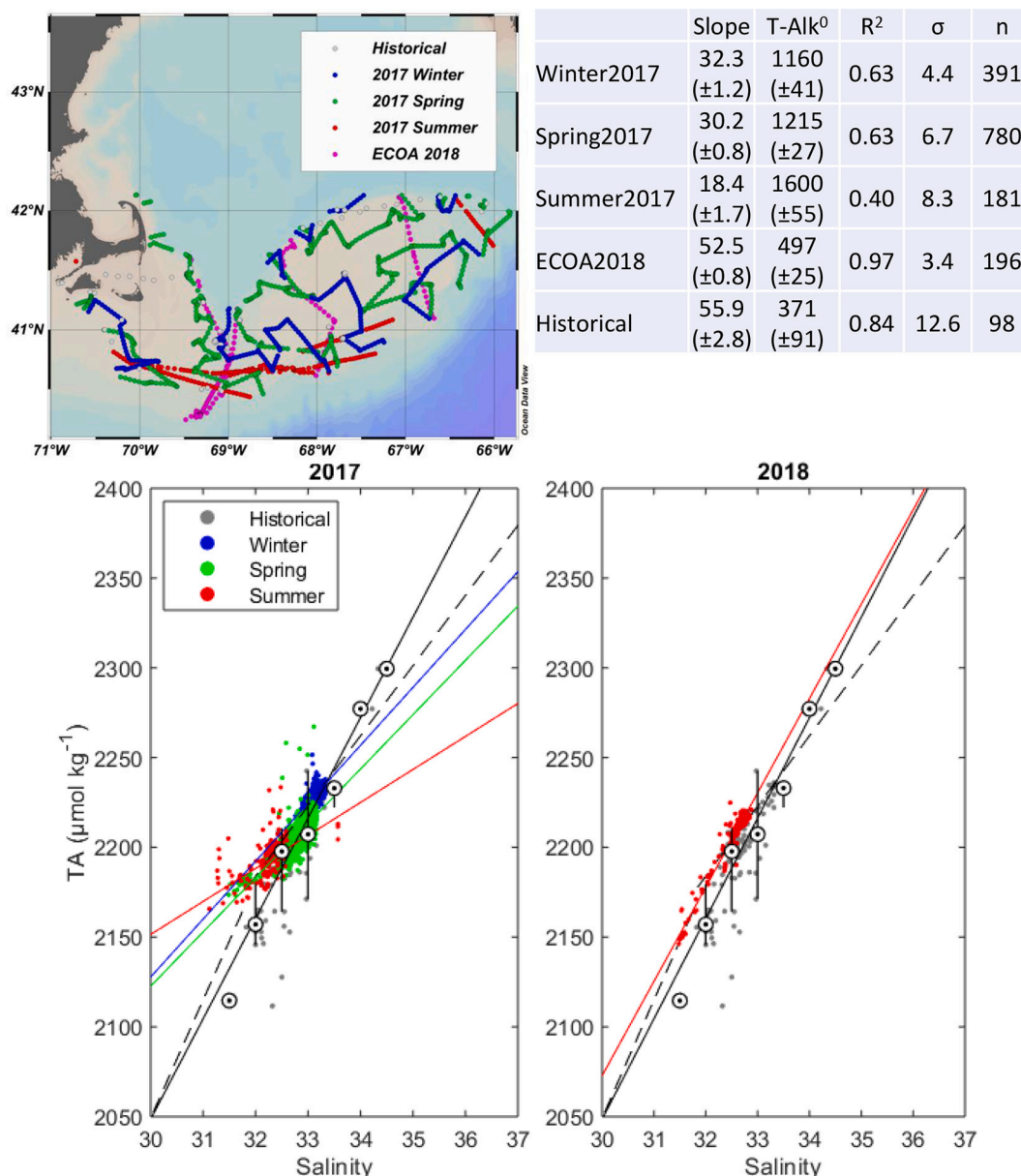


**Fig. 7.** George's Bank-Nantucket Shoals (GBN) seasonal and historic TA and salinity data. See the caption of Fig. 8 for detailed figure explanations. For reference, the solid line indicates the robust linear regression of historical data; the dashed lines indicate the “Woods Hole Transect” mixing lines described by Cai et al. (2010). The slope and TA<sup>0</sup> from Cai et al. (2010) are 73.4 and  $(-188.7 \pm 92.3) \mu\text{mol kg}^{-1}$ , respectively, for sample salinities less than 33. The slope and TA<sup>0</sup> from Cai et al. (2010) are 43.1 and  $809.2 \pm 60.9 \mu\text{mol kg}^{-1}$ , respectively, for sample salinities greater than 33. The p-values for all regressions presented in the table were much less than 0.01.

slope and TA<sup>0</sup> in this study (26.2 and  $1357 \mu\text{mol kg}^{-1}$ , respectively, Fig. 10). As the Labrador Current travels from the Labrador Sea to our study regions and becomes shelf water, it is modified by other inputs, notably those from the St. Lawrence Estuary, which carries massive amounts of freshwater to the Atlantic coast north of Nova Scotia. St. Lawrence Estuary TA<sup>0</sup> ( $1124\text{--}1314 \mu\text{mol kg}^{-1}$ , Dinauer and Mucci 2017, 2018) is typically lower than the TA<sup>0</sup> calculated for spring 2017 in the GOM ( $1415 \mu\text{mol kg}^{-1}$ ) and summer 2017 in all study regions- all TA<sup>0</sup> values which statistically exceed the historical TA<sup>0</sup> for each region by wide margins. Whereas the St. Lawrence experienced a large flooding event in early 2017 (ILO-SLRB 2018), the water transit time of more than six months between the St. Lawrence and the Gulf of Maine discounts the influence of the St. Lawrence on our 2017 observations (Ohashi and Sheng 2013). Measured TA<sup>0</sup> values from local rivers in the GOM, GBN, and MAB regions (Hunt et al. 2011; Cai et al. 2010) are

much too low to account for the elevated TA<sup>0</sup> measured in this study, and discharge levels from these rivers are too small to broadly impact the biogeochemistry of these regions (Cai et al. 2010).

We compared surface salinity measured in this study to climatological data from the World Ocean Atlas 2018 (WOA2018) salinity product (Zweng et al. 2019). Gridded monthly North Atlantic and Coastal WOA2018 salinity at  $1/4^\circ$  resolution was retrieved, and the same regional boundaries discussed previously were used to compute seasonal, climatological statistics for the GOM, GBN, MAB and SBF regions. In three of the four study regions (GOM, GBN, and SBF), the 2017 mean summer salinity was lower than that from winter or spring 2017, and lower than the seasonal mean WOA salinity for winter, spring or summer (see Supplementary Material Fig. S3). The GBN and SBF 2017 mean summer salinities were also lower than those from ECOA-2. The one exception is the MAB region, where the mean 2017 summer salinity was

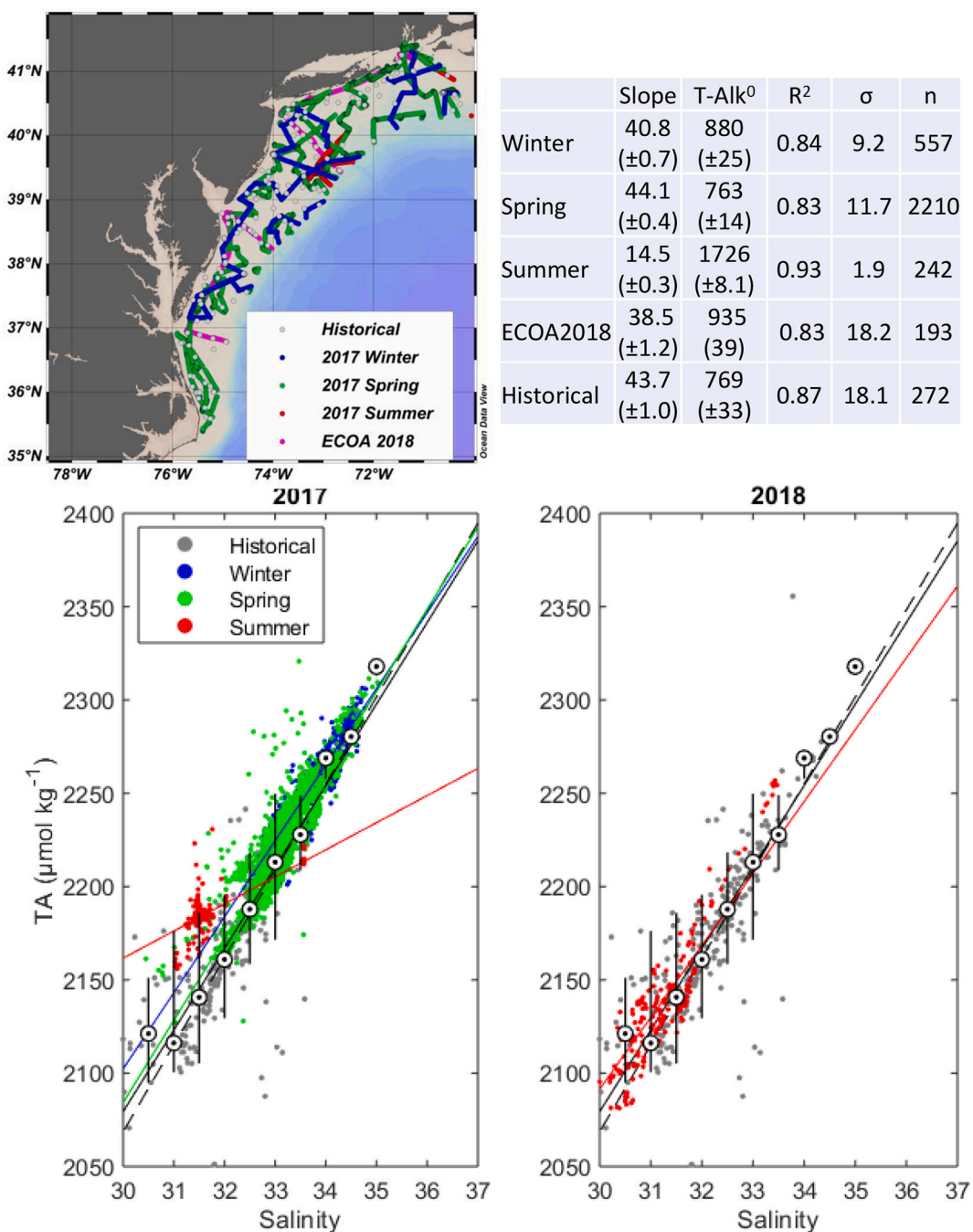


**Fig. 8.** Middle Atlantic Bight (MAB) seasonal and historic TA and salinity data. See the caption of Fig. 8 for detailed figure explanations. For reference, the solid line indicates the robust linear regression of historical data; the dashed line indicates the mixing line described by Cai et al. (2010). The slope and TA<sup>0</sup> from Cai et al. (2010) are 46.6 and  $670.6 \pm 12.3 \mu\text{mol kg}^{-1}$ , respectively. The p-values for all regressions presented in the table were much less than 0.01.

indistinguishable from the mean summer salinity during ECOA-2 or from the WOA, and all were lower than the 2017 mean winter and spring salinities. These exceptionally low salinities show the abnormal levels of freshwater present in the regions, which cannot be accounted for by local river discharge, and instead must be transported southward by upstream sources.

Mixing with freshwater can potentially explain the 2017 changes in TA:S slope but cannot readily explain the relatively low TA at salinities greater than 35, which were observed around Cape Hatteras. Lower than usual pCO<sub>2</sub> suggests that biological uptake through calcification was not likely, and thus another high-salinity endmember, with characteristic TA much lower than the Gulf Stream is needed. One possibility is

provided by Cai et al. (2010), who describe TA:S regressions from seven South Atlantic Bight (SAB) shelf cruises resulting in a calculated TA at salinity 36.5 of 2366–2400  $\mu\text{mol kg}^{-1}$ , with a mean value of 2384  $\mu\text{mol kg}^{-1}$ . The same paper lists an unusual TA:S slope and TA<sup>0</sup> from a series of GYRE93 cruises around the intersection of the MAB and SAB regions which result in an unusually low calculated TA at salinity 36.5 of 2300  $\mu\text{mol kg}^{-1}$ , and support the concept that the observed 2017 TA from this study at salinity 36.5 (2355  $\mu\text{mol kg}^{-1}$ ) is low but not unprecedented. The SAB thus represents a potential high-salinity/low TA water source, through surface water exchange between coastal SAB waters inshore of the Gulf Stream and the MAB and SBF regions, or SBF water transported northwards via the Gulf Stream and then eastwards into the MAB region

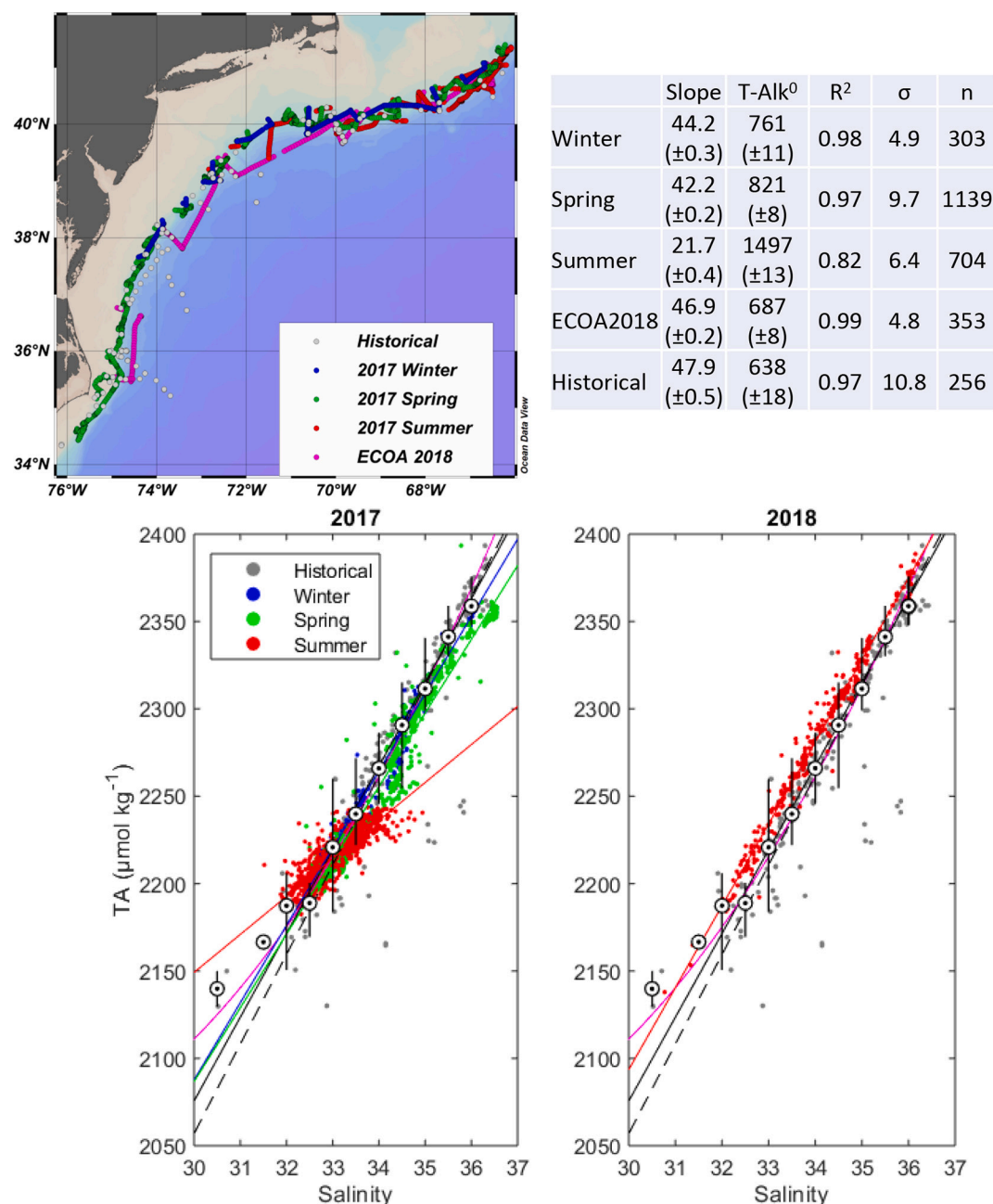


**Fig. 9.** Shelf Break Front (SBF) seasonal and historic TA and salinity data. See the caption of Fig. 8 for detailed figure explanations. For reference, the solid line in the lower two panels indicates the robust linear regression of historical data; the magenta line indicates the mixing line described by Lee et al. (2006,  $TA = 2305 + 53.97*(S - 35) + 2.74*(S - 35)^2 - 1.16(SST - 20) - 0.040(SST - 20)^2$ , where  $S$  is salinity and  $SST$  is surface temperature) and the dashed black line indicates the mixing line described by Millero et al. (1998,  $TA = S*51.24 + 520.1$ , where  $S$  is salinity). The p-values for all regressions presented in the table were much less than 0.01. (For interpretation of the references to colour in this figure legend, the reader is referred to the web version of this article.)

via eddies or warm-core rings (Rasmussen et al. 2005; Hare and Cowen 1996).

Previous work has discussed a mean southward flow of coastal water from the GOM, through the GBN, and into the MAB region (Townsend et al. 2006; Cai et al. 2010; Wang et al. 2013; Wanninkhof et al. 2015), with both salinity and TA enriched by mixing with slope waters along the way. The measurements made as part of this study, as well as the historical data discussed above, indicate that the surface water conditions are substantially more complex between regions and across seasons. In addition to the alongshore gradient in TA, there also appears to be an offshore influence as well, as warmer and saltier north-flowing Gulf Stream water interacts with southward-flowing coastal water masses. The mixing balance between the saltier, TA-enriched

northward-flowing Gulf Stream water, the southward-flowing shelf water, and deeper slope water may dictate much of the distribution of salinity and TA along the East Coast.

#### 4. Conclusions

Deployment of the CONTROS HydroFIA® TA instrument aboard the *Bigelow* produced high quality ( $u_c$  of  $2.4\text{--}4.1\text{ }\mu\text{mol kg}^{-1}$ ) surface TA data over broad spatial and temporal time scales. Results from 2017 and 2018 showed that use of the HydroFIA TA instrument aboard cruises of opportunity can greatly increase regional carbonate system monitoring capacity. Inter-annual and seasonal comparisons showed that TA distributions along the United States East Coast are dynamic, not easily

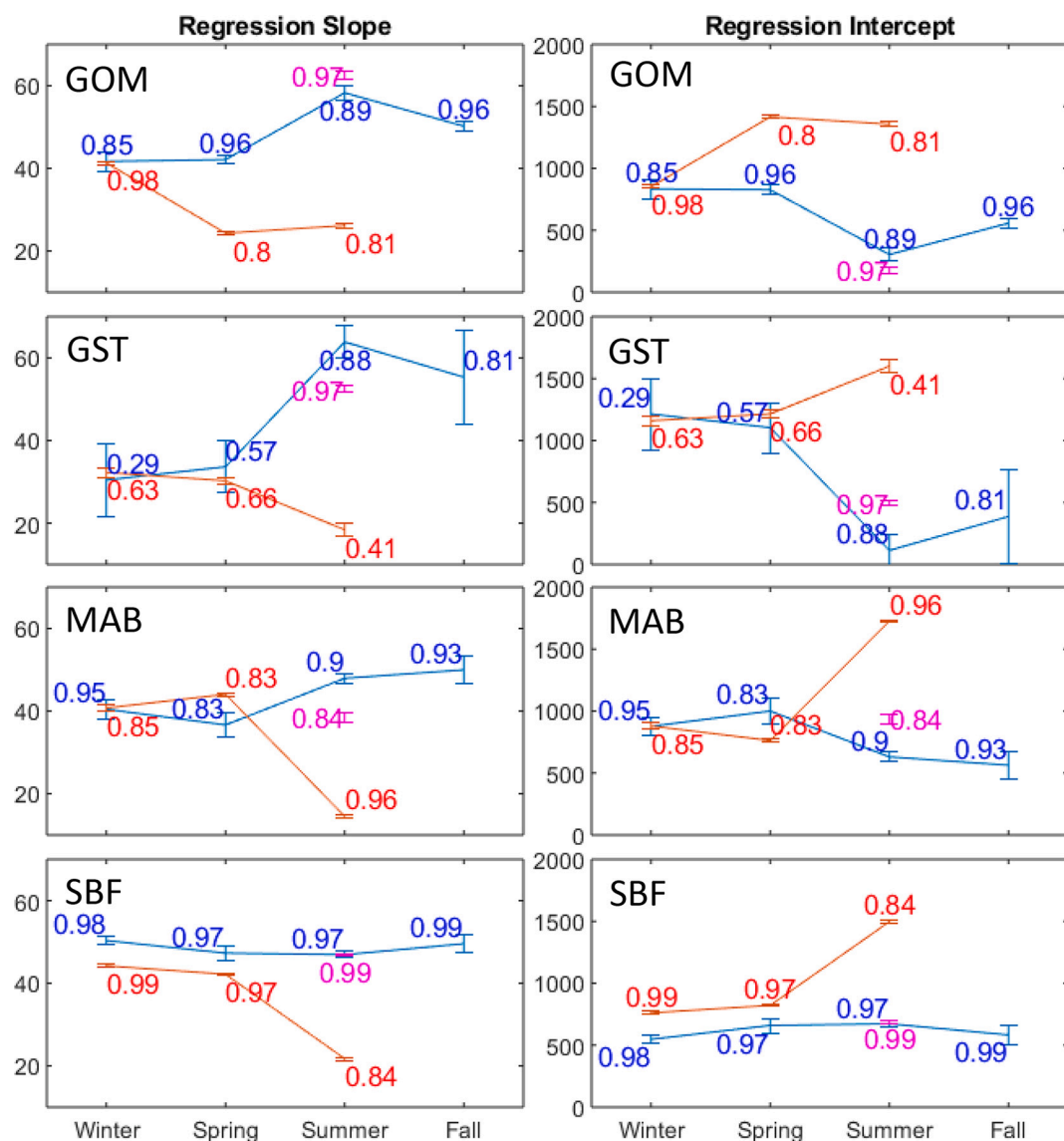


**Fig. 10.** Seasonal, regional slope and y-intercept (TA<sup>0</sup>) statistics produced from a robust linear regression method (see Section 2.3). Error bars show the standard error around each value, and numbers beside each point correspond to the  $r^2$  statistic. Blue lines and  $r^2$  values were calculated from the historical dataset (see Section 2.4), red lines and  $r^2$  values were calculated from the 2017 HydroFIA TA data, and magenta lines and  $r^2$  were calculated from the 2018 ECOA HydroFIA TA data. (For interpretation of the references to colour in this figure legend, the reader is referred to the web version of this article.)

predicted from physical variables such as salinity, and not yet fully characterized by current studies. Significant seasonal shifts in linear TA:S relationships demonstrate potential problems with any single linear model for the retrieval of TA from salinity. Analysis of a compiled historical regional dataset reinforces the finding that salinity, TA, and TA:S linear relationships shift seasonally, although data availability is extremely sparse in some months and regions. Additional deployments during undersampled months may further advance the understanding of the seasonal nature of TA:S relationship in these regions, and analyses of derived DIC, pH or carbonate saturation state may provide even more insights. Especially when deployed on ships equipped with instrumentation to measure another carbonate system parameter (i.e. pCO<sub>2</sub>), the HydroFIA TA instrument represents a substantial advancement in the ability to comprehensively monitor and characterize surface waters.

#### Declaration of Competing Interest

None.

#### Acknowledgements

This work was supported by NOAA TTP Project NA15NOS0120155-Tracking Ocean Alkalinity using New Carbon Measurement Technologies (TAACT). The comments provided by three reviewers and Associate Editor A. Mucci were invaluable in improving this work. We gratefully acknowledge the extensive shipboard and laboratory assistance of Christopher Taylor, Mark Bradley, Marc Emond, Katherine McGinnis, and Shawn Shellito, Denis Pierrot of AOML for providing pCO<sub>2</sub> data, and the incomparable support provided by Jacob Sabin of Kongsberg Underwater Technology, LLC.

#### Appendix A. Supplementary data

Supplementary data to this article can be found online at <https://doi.org/10.1016/j.marchem.2021.103960>.

## References

AOML, 2020. HB1701 Cruise Report. Accessed September 25. <https://www.aoml.noaa.gov/ocd/gcc/shortcruises/HB1701/33H20170210-HB1701-Readme.pdf>.

Åbmann, S., Frank, C., Petersen, W., Körtzinger, A., 2013. Autonomous pH and alkalinity sensors for the characterization of the carbonate system in coastal areas. In: Presented at the EGU General Assembly Conference Abstracts. EGU2013-8760.

Bakker, D.C.E., Pfeil, B., Land, C.S., Metzl, N., O'Brien, K.M., Olsen, A., Smith, K., Cosca, C., Harasawa, S., Jones, S.D., Nakaoaka, S., Nojiri, Y., Schuster, U., Steinhoff, T., Sweeney, C., Takahashi, T., Tilbrook, B., Wada, C., Wanninkhof, R., Alin, S.R., Balestrini, C.F., Barbero, L., Bates, N.R., Bianchi, A.A., Bonou, F., Boutin, J., Bozec, Y., Burger, E.F., Cai, W.-J., Castle, R.D., Chen, L., Chierici, M., Currie, K., Evans, W., Featherstone, C., Feely, R.A., Fransson, A., Goyet, C., Greenwood, N., Gregor, L., Hankin, S., Hardman-Mountford, N.J., Harley, J., Hauck, J., Hoppema, M., Humphreys, M.P., Hunt, C.W., Huss, B., Ibáñez, J.S.P., Johannessen, T., Keeling, R., Kitidis, V., Körtzinger, A., Kozyr, A., Krasakopoulou, E., Kuwata, A., Landschützer, P., Lauvset, S.K., Lefèvre, N., Monaco, C.L., Manke, A., Mathis, J.T., Merlin, L., Millero, F.J., Monteiro, P.M.S., Munro, D.R., Murata, A., Newberger, T., Omar, A.M., Ono, T., Paterson, K., Pearce, D., Pierrot, D., Robbins, L., Saito, S., Salisbury, J., Schlitzer, R., Schneider, B., Schweitzer, R., Sieger, R., Skjelvan, I., Sullivan, K.F., Sutherland, S.C., Sutton, A.J., Tadokoro, K., Telszewski, M., Tuma, M., Heuven, S.M.A.C., Vandemark, D., Ward, B., Watson, A.J., Xu, S., 2016. A multi-decade record of high-quality pCO<sub>2</sub> data in version 3 of the Surface Ocean CO<sub>2</sub> atlas (SOCAT). *Earth Syst. Sci. Data* 8, 383–413. <https://doi.org/10.5194/essd-8-383-2016>

Balch, W.M. 2018. The ecology, biogeochemistry, and optical properties of coccolithophores. *Annu. Rev. Mar. Sci.* 10, 71–98. doi:10.1146/annurev-marine-121916-063319.

Barbero, L., Pierrot, D., Wanninkhof, R., et al., 2017. Third gulf of mexico ecosystems and carbon cycle (GOMECC-3) Cruise. In: Cruise Report. <https://doi.org/10.25923/y6m9-fy08>.

Bates, N.R., 2001. Interannual variability of oceanic CO<sub>2</sub> and biogeochemical properties in the Western North Atlantic subtropical gyre. *Deep-Sea Res. II Top. Stud. Oceanogr.* 48, 1507–1528. [https://doi.org/10.1016/S0967-0645\(00\)00151-X](https://doi.org/10.1016/S0967-0645(00)00151-X).

Bates, N.R., Michaels, A.F., Knap, A.H., 1996a. Seasonal and interannual variability of oceanic carbon dioxide species at the U.S. JGOFS Bermuda Atlantic Time-series Study (BATS) site. *Deep-Sea Res. II Top. Stud. Oceanogr.* 43, 347–383. [https://doi.org/10.1016/0967-0645\(95\)00093-3](https://doi.org/10.1016/0967-0645(95)00093-3).

Bates, N.R., Michaels, A.F., Knap, A.H., 1996b. Alkalinity changes in the Sargasso Sea: geochemical evidence of calcification? *Mar. Chem.* 51, 347–358. [https://doi.org/10.1016/0304-4203\(95\)00068-2](https://doi.org/10.1016/0304-4203(95)00068-2).

Breitburg, D.L., Salisbury, J., Bernhard, J.M., Cai, W.-J., Dupont, S., Doney, S.C., Kroeker, K.J., Levin, L.A., Long, W.C., Milke, L.M., Miller, S.H., Phelan, B., Passow, U., Seibel, B.A., Todgham, A.E., Tarrant, A.M., 2015. And on top of all that...: coping with ocean acidification in the midst of many stressors. *Oceanography* 28, 48–61.

Brickman, D., Hebert, D., Wang, Z., 2018. Mechanism for the recent ocean warming events on the Scotian Shelf of eastern Canada. *Cont. Shelf Res.* 156, 11–22. <https://doi.org/10.1016/j.csr.2018.01.001>.

Cai, W.-J., Hu, X., Huang, W.-J., Jiang, L.-Q., Wang, Y., Peng, T.-H., Zhang, X., 2010. Alkalinity distribution in the western North Atlantic Ocean margins. *J. Geophys. Res.* 115 <https://doi.org/10.1029/2009JC005482>. C08014.

Cai, W.-J., Hu, X., Huang, W.-J., others, 2011. Acidification of subsurface coastal waters enhanced by eutrophication. *Nat. Geosci.* 4, 766–770. <https://doi.org/10.1038/geo1297>.

Chen, C.-T.A., Wang, S.-L., 1999. Carbon, alkalinity and nutrient budgets on the East China Sea continental shelf. *J. Geophys. Res. Oceans* 104, 20675–20686. <https://doi.org/10.1029/1999JC900055>.

Chipman, D.W., Sutherland, S.C., Takahashi, T., 1995. Determination of ocean/atmosphere carbon dioxide flux within the OMP study area. In: Final Technical Report for Grant DE-FG02-92ER61451. Observatory of Columbia University, Lamont-Doherty (16 pp).

Claret, M., Galbraith, E.D., Palter, J.B., Bianchi, D., Fennel, K., Gilbert, D., Dunne, J.P., 2018. Rapid coastal deoxygenation due to ocean circulation shift in the Northwest Atlantic. *Nat. Clim. Chang.* 8, 868–872. <https://doi.org/10.1038/s41558-018-0263-1>.

Cross, J.N., Mathis, J.T., Bates, N.R., Byrne, R.H., 2013. Conservative and non-conservative variations of total alkalinity on the southeastern Bering Sea shelf. *Mar. Chem.* 154, 100–112. <https://doi.org/10.1016/j.marchem.2013.05.012>.

DeGrandpre, M.D., Hammar, T.R., Wallace, D.W.R., Wirick, C.D., 1997. Simultaneous mooring-based measurements of seawater CO<sub>2</sub> and O<sub>2</sub> off Cape Hatteras, North Carolina. *Limnol. Oceanogr.* 42, 21–28. <https://doi.org/10.4319/lo.1997.42.1.0021>.

DeGrandpre, M.D., Olbu, G.J., Beatty, C.M., Hammar, T.R., 2002. Air-sea CO<sub>2</sub> fluxes on the US middle Atlantic bight: deep sea research part II: topical studies in oceanography, carbon cycling and biogeochemistry in the Northwest Atlantic Shelf slope: results of the ocean margins. *Program* 49, 4355–4367. [https://doi.org/10.1016/S0967-0645\(02\)00122-4](https://doi.org/10.1016/S0967-0645(02)00122-4).

Dickson, A.G., 1981. An exact definition of total alkalinity and a procedure for the estimation of alkalinity and total inorganic carbon from titration data. *Deep Sea Res. Part A. Oceanogr. Res. Papers* 28, 609–623. [https://doi.org/10.1016/0198-0149\(81\)90121-7](https://doi.org/10.1016/0198-0149(81)90121-7).

Dickson, A.G., Afghan, J.D., Anderson, G.C., 2003. Reference materials for oceanic CO<sub>2</sub> analysis: a method for the certification of total alkalinity. *Mar. Chem.* 80, 185–197. [https://doi.org/10.1016/S0304-4203\(02\)00133-0](https://doi.org/10.1016/S0304-4203(02)00133-0).

Dickson, A.G., Sabine, C.L., Christian, J.R. (Eds.), 2007. *Guide to Best Practices for Ocean CO<sub>2</sub> Measurements*, 3. PICES Special Publication, 191 pp.

Dinauer, A., Mucci, A., 2017. Spatial variability in surface-water pCO<sub>2</sub> and gas exchange in the world's largest semi-enclosed estuarine system: St. Lawrence Estuary (Canada). *Biogeosciences* 14, 3221–3237. <https://doi.org/10.5194/bg-14-3221-2017>.

Dinauer, A., Mucci, A., 2018. Distinguishing between physical and biological controls on the spatial variability of pCO<sub>2</sub>: a novel approach using OMP water mass analysis (St. Lawrence, Canada). *Mar. Chem.* 204, 107–120.

Doney, S.C., Ruckelshaus, M., Emmett Duffy, J., Barry, J.P., Chan, F., English, C.A., Galindo, H.M., Grebmeier, J.M., Hollowed, A.B., Knowlton, N., Polovina, J., Rabalais, N.N., Sydeman, W.J., Talley, L.D., 2011. Climate change impacts on marine ecosystems. *Annu. Rev. Mar. Sci.* 4, 11–37. <https://doi.org/10.1146/annurev-marine-041911-111611>.

Dupont, F., Hannah, C.G., Wright, D.G., 2006. Model investigation of the slope water, north of the Gulf stream. *Geophys. Res. Lett.* 33 <https://doi.org/10.1029/2005GL025321>.

Feely, R.A., Sabine, C.L., Lee, K., Berelson, W., Kleypas, J., Fabry, V.J., Millero, F.J., 2004. Impact of anthropogenic CO<sub>2</sub> on the CaCO<sub>3</sub> system in the oceans. *Science* 305, 362–366. <https://doi.org/10.1126/science.1097329>.

Fine, R.A., Willey, D.A., Millero, F.J., 2017. Global variability and changes in ocean total alkalinity from Aquarius satellite data. *Geophys. Res. Lett.* 44, 261–267. <https://doi.org/10.1002/2016GL071712>.

Fong, M.B., Dickson, A.G., 2019. Insights from GO-SHIP hydrography data into the thermodynamic consistency of CO<sub>2</sub> system measurements in seawater. *Mar. Chem.* 211, 52–63. <https://doi.org/10.1016/j.marchem.2019.03.006>.

Friedlingstein, P., Jones, M.W., O'Sullivan, M., Andrew, R.M., Hauck, J., Peters, G.P., Peters, W., Ponratz, J., Sitch, S., Quéré, C.L., Bakker, D.C.E., Canadell, J.G., Ciais, P., Jackson, R.B., Anthoni, P., Barbero, L., Bastos, A., Bastrikov, V., Becker, M., Bopp, L., Buitenhuis, E., Chandra, N., Chevallier, F., Chini, L.P., Currie, K.I., Feely, R.A., Gehlen, M., Gilfillan, D., Grätzalis, T., Goll, D.S., Gruber, N., Gutekunst, S., Harris, I., Haverd, V., Houghton, R.A., Hurt, G., Ilyina, T., Jain, A.K., Joetzjer, E., Kaplan, J.O., Kato, E., Klein, Goldeijk, K., Korsbakken, J.I., Landschützer, P., Lauvset, S.K., Lefèvre, N., Lenten, A., Lienert, S., Lombardozzi, D., Marland, G., McGuire, P.C., Melton, J.R., Metzl, N., Munro, D.R., Nabel, J.E.M.S., Nakaoaka, S.-I., Neill, C., Omar, A.M., Ono, T., Peregon, A., Pierrot, D., Poulet, B., Rehder, G., Resplandy, L., Robertson, E., Rödenbeck, C., Séferian, R., Schwinger, J., Smith, N., Tans, P.P., Tian, H., Tilbrook, B., Tubiello, F.N., van der Werf, G.R., Wiltshire, A.J., Zeehle, S., 2019. Global carbon budget 2019. *Earth Syst. Sci. Data* 11, 1783–1838. <https://doi.org/10.5194/essd-11-1783-2019>.

Fry, C.H., Tyrrell, T., Hain, M.P., Bates, N.R., Achterberg, E.P., 2015. Analysis of global surface ocean alkalinity to determine controlling processes. *Mar. Chem.* 174, 46–57. <https://doi.org/10.1016/j.marchem.2015.05.003>.

Gran, G., 1952. Determination of the equivalence point in potentiometric titrations. Part II. *Analyst* 77, 661–671. <https://doi.org/10.1039/AN9527700661>.

Grodsky, S.A., Vandemark, D., Feng, H., Levin, J., 2018. Satellite detection of an unusual intrusion of salty slope water into a marginal sea: using SMAP to monitor gulf of Maine inflows. *Remote Sens. Environ.* 217, 550–561. <https://doi.org/10.1016/j.rse.2018.09.004>.

Hagens, M., Slomp, C.P., Meysman, F.J.R., Seitaj, D., Harlay, J., Borges, A.V., Middelburg, J.J., 2015. Biogeochemical processes and buffering capacity concurrently affect acidification in a seasonally hypoxic coastal marine basin. *Biogeosciences* 12, 1561–1583. <https://doi.org/10.5194/bg-12-1561-2015>.

Hare, J.A., Cowen, R.K., 1996. Transport mechanisms of larval and pelagic juvenile bluefish (*Pomatomus saltatrix*) from South Atlantic bight spawning grounds to middle Atlantic bight nursery habitats. *Limnol. Oceanogr.* 41, 1264–1280. <https://doi.org/10.4319/lo.1996.41.6.1264>.

Harlay, J., Borges, A.V., Van Der Zee, C., Delille, B., Godoi, R.H.M., Schiettecatte, L.S., Roevros, N., Aerts, K., Lapernat, P.-E., Rebreau, L., Groom, S., Daro, M.-H., Van Grieken, R., Chou, L., 2010. Biogeochemical study of a coccolithophore bloom in the northern Bay of Biscay (NE Atlantic Ocean) in June 2004. *Prog. Oceanogr.* 86, 317–336. <https://doi.org/10.1016/j.pocean.2010.04.029>.

Hofmann, E., Druon, J.-N., Fennel, K., Friedrichs, M., Haidvogel, D., Lee, C., Mannino, A., McClain, C., Najar, R., O'Reilly, J., Pollard, D., Previdi, M., Seitzinger, S., Siewert, J., Signorini, S., Wilkin, J., 2008. Eastern US continental shelf carbon budget: integrating models, data assimilation, and analysis. *Oceanography* 21, 86–104. <https://doi.org/10.5670/oceanog.2008.70>.

Hunt, C.W., Salisbury, J.E., Vandemark, D., 2011. Contribution of non-carbonate anions to total alkalinity and overestimation of pCO<sub>2</sub> in New England and New Brunswick rivers. *Biogeosciences* 8, 3069–3076. <https://doi.org/10.5194/bg-8-3069-2011>.

(ILO-SLRB) International Lake Ontario-St., 2018. Lawrence River Board. 2018. Lake Ontario - St. Lawrence River 2017 High Water - Questions and Answers. International Joint Commission. <https://ijc.org/en/losrb/watershed/faq/2017> (Accessed 10/5/2020).

Jiang, Z.-P., Tyrrell, T., Hydes, D.J., Dai, M., Hartman, S.E., 2014. Variability of alkalinity and the alkalinity-salinity relationship in the tropical and subtropical surface ocean. *Glob. Biogeochem. Cycles* 28, 729–742. <https://doi.org/10.1002/2013GB004678>.

Joesoef, A., Kirchman, D.L., Sommerfield, C.K., Cai, W.-J., 2017. Seasonal variability of the inorganic carbon system in a large coastal plain estuary. *Biogeosciences* 14, 4949–4963. <https://doi.org/10.5194/bg-14-4949-2017>.

Jutras, M., Dufour, C.O., Mucci, A., Cyr, F., Gilbert, D., 2020. Temporal changes in the causes of the observed oxygen decline in the St. Lawrence Estuary. *J. Geophys. Res. Oceans* 125. <https://doi.org/10.1029/2020JC016577> e2020JC016577.

Key, R.M., Olsen, A., van Heuven, S., Lauvset, S.K., Velo, A., Lin, X., Schirnick, C., Kozyr, A., Tanhua, T., Hoppema, M., Jutterström, S., Steinfeldt, R., Jeansson, E., Ishii, M., Perez, F.F., Suzuki, T., 2015. Global Ocean Data Analysis Project, Version 2 (GLODAPv2), ORNL/CDIAC-162, ND-P093. Carbon Dioxide Information Analysis Center, Oak Ridge National Laboratory, US Department of Energy, Oak Ridge, Tennessee. [https://doi.org/10.3334/CDIAC/OTG.NDP093\\_GLODAPv2](https://doi.org/10.3334/CDIAC/OTG.NDP093_GLODAPv2).

Kulinski, K., Schneider, B., Hammer, K., Machulik, U., Schulz-Bull, D., 2014. The influence of dissolved organic matter on the acid-base system of the Baltic Sea. *J. Mar. Syst.* 132, 106–115. <https://doi.org/10.1016/j.jmarsys.2014.01.011>.

Land, P.E., Findlay, H.S., Shutler, J.D., Ashton, I.G.C., Holding, T., Grouazel, A., Girard-Ardhuin, F., Reul, N., Piole, J.-F., Chapron, B., Quilfen, Y., Bellerby, R.G.J., Bhadury, P., Salisbury, J., Vandemark, D., Sabia, R., 2019. Optimum satellite remote sensing of the marine carbonate system using empirical algorithms in the global ocean, the greater Caribbean, the Amazon plume and the bay of Bengal. *Remote Sens. Environ.* 235, 111469. <https://doi.org/10.1016/j.rse.2019.111469>.

Lee, K., Tong, L.T., Millero, F.J., Sabine, C.L., Dickson, A.G., Goyet, C., Park, G.-H., Wanninkhof, R., Feely, R.A., Key, R.M., 2006. Global relationships of total alkalinity with salinity and temperature in surface waters of the world's oceans. *Geophys. Res. Lett.* 33. <https://doi.org/10.1029/2006GL027207>.

Li, Q., Wang, F., Wang, Z.A., Yuan, D., Dai, M., Chen, J., Dai, J., Hoering, K.A., 2013. Automated spectrophotometric analyzer for rapid single-point titration of seawater total alkalinity. *Environ. Sci. Technol.* 47, 11139–11146. <https://doi.org/10.1021/es402421a>.

Li, X., Bellerby, R.G.J., Wallhead, P., Ge, J., Liu, Jie, Liu, Jing, Yang, A., 2020. A neural network-based analysis of the seasonal variability of surface total alkalinity on the East China Sea shelf. *Front. Mar. Sci.* 7. <https://doi.org/10.3389/fmars.2020.00219>.

Loder, J.W., 1998. The coastal ocean off northeastern North America: a large-scale view. *The Sea* 11, 105–138.

Mathis, J., Cross, J., Evans, W., Doney, S., 2015. Ocean acidification in the surface waters of the Pacific-Arctic boundary regions. *Oceanography* 25, 122–135. <https://doi.org/10.5670/oceanog.2015.36>.

Millero, F.J., Lee, K., Roche, M., 1998. Distribution of alkalinity in the surface waters of the major oceans. *Mar. Chem.* 60, 111–130. [https://doi.org/10.1016/S0304-4203\(97\)00084-4](https://doi.org/10.1016/S0304-4203(97)00084-4).

Mucci, A., Starr, M., Gilbert, D., Sundby, B., 2011. Acidification of lower St. Lawrence estuary bottom waters. *Atmosphere-Ocean* 49, 206–218. <https://doi.org/10.1080/07055900.2011.599265>.

Ohashi, K., Sheng, J., 2013. Influence of St. Lawrence River discharge on the circulation and hydrography in Canadian Atlantic waters. *Cont. Shelf Res.* 58, 32–49. <https://doi.org/10.1016/j.csr.2013.03.005>.

Olsen, A., Key, R.M., Heuven, S., Lauvset, S.K., Velo, A., Lin, X., Schirnick, C., Kozyr, A., Tanhua, T., Hoppema, M., Jutterström, S., Steinfeldt, R., Jeansson, E., Ishii, M., Pérez, F.F., Suzuki, T., 2016. The Global Ocean data analysis project version 2 (GLODAPv2) – an internally consistent data product for the world ocean. *Earth Syst. Sci. Data* 8, 297–323. <https://doi.org/10.5194/essd-8-297-2016>.

Pershing, A.J., Alexander, M.A., Hernandez, C.M., et al., 2015. Slow adaptation in the face of rapid warming leads to collapse of the Gulf of Maine cod fishery. *Science* 350, 809–812. <https://doi.org/10.1126/science.aac9819>.

Pershing, A., Dayton, A., Franklin, B., Kennedy, B., 2018. Evidence for adaptation from the 2016 marine Heatwave in the Northwest Atlantic Ocean. *Oceanogr* 31. <https://doi.org/10.5670/oceanog.2018.213>.

Pierrot, D., Neill, C., Sullivan, K., Castle, R., Wanninkhof, R., Lüger, H., Johannessen, T., Olsen, A., Feely, R.A., Cosca, C.E., 2009. Recommendations for autonomous underway pCO<sub>2</sub> measuring systems and data-reduction routines. Deep Sea research part II: topical studies in oceanography. *Surface Ocean CO<sub>2</sub> Variabil. Vulnerabilit.* 56, 512–522. <https://doi.org/10.1016/j.dsr2.2008.12.005>.

Rasmussen, L.L., Gawarkiewicz, G., Owens, W.B., Lozier, M.S., 2005. Slope water, gulf stream, and seasonal influences on southern mid-Atlantic bight circulation during the fall-winter transition. *J. Geophys. Res. Oceans* 110. <https://doi.org/10.1029/2004JC002311>.

Reul, N., Grodsky, S.A., Arias, M., Boutin, J., Catany, R., Chapron, B., D'Amico, F., Dinnat, E., Donlon, C., Fore, A., Fournier, S., Guimbard, S., Hasson, A., Kolodziejczyk, N., Lagerloef, G., Lee, T., Le Vine, D.M., Lindstrom, E., Maes, C., Mecklenburg, S., Meissner, T., Olmedo, E., Sabia, R., Tenerelli, J., Thouvenin-Masson, C., Turiel, A., Vergely, J.L., Vinogradova, N., Wentz, F., Yueh, S., 2020. Sea surface salinity estimates from spaceborne L-band radiometers: an overview of the first decade of observation (2010–2019). *Remote Sens. Environ.* 242, 111769. <https://doi.org/10.1016/j.rse.2020.111769>.

Salisbury, J.E., Jönsson, B.F., 2018. Rapid warming and salinity changes in the Gulf of Maine alter surface ocean carbonate parameters and hide ocean acidification. *Biogeochemistry* 141, 401–418. <https://doi.org/10.1007/s10533-018-0505-3>.

Salisbury, J., Green, M., Hunt, C., Campbell, J., 2008. Coastal acidification by rivers: a threat to shellfish? *Eos Trans. AGU* 89, 513. <https://doi.org/10.1029/2008EO500001>.

Salisbury, J., Vandemark, D., Jönsson, B., Balch, W., Chakraborty, S., Lohrenz, S., Chapron, B., Hales, B., Mannino, A., Mathis, J., Reul, N., Signorini, S., Wanninkhof, R., Yates, K., 2015. How can present and future satellite missions support scientific studies that address ocean acidification? *Oceanography* 25, 108–121. <https://doi.org/10.5670/oceanog.2015.35>.

Seelmann, K., Aßmann, S., Körtzinger, A., 2019. Characterization of a novel autonomous analyzer for seawater total alkalinity: results from laboratory and field tests. *Limnol. Oceanogr. Methods* 17, 515–532. <https://doi.org/10.1002/lom3.10329>.

Sharp, J.D., Byrne, R.H., 2020. Interpreting measurements of total alkalinity in marine and estuarine waters in the presence of proton-binding organic matter. *Deep-Sea Res. I Oceanogr. Res. Pap.* 165, 103338. <https://doi.org/10.1016/j.dsr.2020.103338>.

Sherwood, O.A., Lehmann, M.F., Schubert, C.J., Scott, D.B., McCarthy, M.D., 2011. Nutrient regime shift in the western North Atlantic indicated by compound-specific <sup>81</sup>IN of deep-sea gorgonian corals. *PNAS* 108, 1011–1015. <https://doi.org/10.1073/pnas.1004904108>.

Signorini, S.R., Mannino, A., Najjar, R.G., Friedrichs, M.A.M., Cai, W.-J., Salisbury, J., Wang, Z.A., Thomas, H., Shadwick, E., 2013. Surface ocean pCO<sub>2</sub> seasonality and sea-air CO<sub>2</sub> flux estimates for the north American east coast. *J. Geophys. Res. Oceans* 118, 5439–5460. <https://doi.org/10.1002/jgrc.20369>.

Takahashi, T., Sutherland, S.C., Chipman, D.W., Goddard, J.G., Ho, C., Newberger, T., Sweeney, C., Munro, D.R., 2014. Climatological distributions of pH, pCO<sub>2</sub>, total CO<sub>2</sub>, alkalinity, and CaCO<sub>3</sub> saturation in the global surface ocean, and temporal changes at selected locations. *Mar. Chem.* 164, 95–125. <https://doi.org/10.1016/j.marchem.2014.06.004>.

Thomas, H., Schiettecatte, L.-S., Suykens, K., Koné, Y.J.M., Shadwick, E.H., Prowe, A.E. F., Bozec, Y., de Baar, H.J.W., Borges, A.V., 2009. Enhanced ocean carbon storage from anaerobic alkalinity generation in coastal sediments. *Biogeosciences* 6, 267–274. <https://doi.org/10.5194/bg-6-267-2009>.

Townsend, D.W., Thomas, A.C., Mayer, L.M., Thomas, M., Quinlan, J., 2006. *Oceanography of the Northwest Atlantic continental shelf*. In: *The Sea*. Harvard University Press, pp. 119–168.

Townsend, D.W., Pettigrew, N.R., Thomas, M.A., Neary, M.G., McGillicuddy, D.J., O'Donnell, J., 2015. Water masses and nutrient sources to the Gulf of Maine. *J. Mar. Res.* 73, 93–122. <https://doi.org/10.1357/00224015815848811>.

Wallace, R.B., Baumann, H., Grear, J.S., Aller, R.C., Gobler, C.J., 2014. Coastal Ocean acidification: the other eutrophication problem. *Estuar. Coast. Shelf Sci.* 148, 1–13. <https://doi.org/10.1016/j.ecss.2014.05.027>.

Wang, Z.A., Wanninkhof, R., Cai, W.-J., Byrne, R.H., Hu, X., Peng, T.-H., Huang, W.-J., 2013. The marine inorganic carbon system along the Gulf of Mexico and Atlantic coasts of the United States: insights from a transregional coastal carbon study. *Limnol. Oceanogr.* 58, 325–342. <https://doi.org/10.4319/lo.2013.58.1.0325>.

Wang, Z.A., Kroeger, K.D., Ganju, N.K., Gonnea, M.E., Chu, S.N., 2016. Intertidal salt marshes as an important source of inorganic carbon to the coastal ocean. *Limnol. Oceanogr.* 61, 1916–1931. <https://doi.org/10.1002/lo.10347>.

Wanninkhof, R., Barbero, L., Byrne, R., Cai, W.-J., Huang, W.-J., Zhang, J.-Z., Baringer, M., Langdon, C., 2015. Ocean acidification along the Gulf Coast and East Coast of the USA. *Cont. Shelf Res.* 98, 54–71. <https://doi.org/10.1016/j.csr.2015.02.008>.

Xu, Y.-Y., Cai, W.-J., Gao, Y., et al., 2017. Short-term variability of aragonite saturation state in the central Mid-Atlantic Bight. *J. Geophys. Res. Oceans* 122, 4274–4290. <https://doi.org/10.1002/2017JC012901>.

Yang, B., Byrne, R.H., Lindemuth, M., 2015. Contributions of organic alkalinity to total alkalinity in coastal waters: a spectrophotometric approach. *Mar. Chem.* 176, 199–207. <https://doi.org/10.1016/j.marchem.2015.09.008>.

Yao, W., Byrne, R.H., 1998. Simplified seawater alkalinity analysis. *Deep-Sea Res. I Oceanogr. Res. Pap.* 45, 1383–1392. [https://doi.org/10.1016/S0967-0637\(98\)00018-1](https://doi.org/10.1016/S0967-0637(98)00018-1).

Zeebe, R.E., 2012. History of seawater carbonate chemistry, atmospheric CO<sub>2</sub>, and ocean acidification. *Annu. Rev. Earth Planet. Sci.* 40, 141–165. <https://doi.org/10.1146/annurev-earth-042711-105521>.

Zweng, M.M., Reagan, J.R., Seidov, D., Boyer, T.P., Locarnini, R.A., Garcia, H.E., Mishonov, A.V., Baranova, O.K., Weathers, K.W., Paver, C.R., Smolyar, I.V., 2019. In: Mishonov, A. (Ed.), *World Ocean Atlas 2018, Volume 2: Salinity*. NOAA Atlas NESDIS 82. Technical Editor. 50pp.